Fatty acid uptake activates an AXL–CAV1–β-catenin axis to drive melanoma progression

Ana Chocarro-Calvo,[1,2,6] Miguel Jociles-Ortega,[2,6] José Manuel García-Martinez,[2] Pakavarin Louphrasitthiphol,[1] Sofia Carvalho-Marques,[3] Yurena Vivas-García,[1] Ana Ramírez-Sánchez,[2] Jagat Chauhan,[1] M. Carmen Fiuza,[4] Manuel Duran,[5] Adriana Sánchez-Danés,[3] Colin R. Goding,[1] and Custodia García-Jiménez[2]

[1]Ludwig Institute for Cancer Research, Nuffield Department of Clinical Medicine, University of Oxford, Headington, Oxford OX3 7DQ, United Kingdom; [2]Area of Physiology, Faculty Health Sciences, University Rey Juan Carlos, Alcorcón, Madrid 28922, Spain; [3]Champalimaud Research, Champalimaud Centre for the Unknown, 1400-038 Lisboa, Portugal; [4]Department of Surgery, University Hospital Fundación Alcorcón, Alcorcón, Madrid 28922, Spain; [5]Department of General Surgery, University Hospital Rey Juan Carlos, Móstoles, Madrid 28933, Spain

Interaction between the tumor microenvironment and cancer cell plasticity drives intratumor phenotypic heterogeneity and underpins disease progression and nongenetic therapy resistance. Phenotype-specific expression of the AXL receptor tyrosine kinase is a pivotal player in dormancy, invasion, and resistance to treatment. However, although the AXL ligand GAS6 is present within tumors, how AXL is activated in metastasizing cells remains unclear. Here, using melanoma as a model, we reveal that AXL is activated by exposure to human adipocytes and to oleic acid, a monounsaturated fatty acid abundant in lymph and in adipocytes. AXL activation triggers SRC-dependent formation and nuclear translocation of a β-catenin–CAV1 complex required for melanoma invasiveness. Remarkably, only undifferentiated AXL^{High} melanoma cells engage in symbiosis with human adipocytes, in part by triggering WNT5a-mediated lipolysis, leading to AXL-dependent, but FATP-independent, fatty acid uptake and nuclear localization of the β-catenin–CAV1 complex. Significantly, human melanomas in the vicinity of adipocytes exhibit high levels of nuclear CAV1. The results unveil an AXL- and CAV1-dependent mechanism through which a nutritional input drives phenotype-specific activation of a prometastasis program. Given the key role of AXL in a broad range of cancers, the results offer major insights into the mechanisms of cancer cell dormancy and therapy resistance.

[*Keywords*: adipocytes; melanoma; SRC; AXL; oleic acid; β-catenin; caveolin; WNT5A]

Supplemental material is available for this article.

Received June 3, 2024; revised version accepted January 27, 2025.

Tumors contain multiple phenotypically distinct cell subpopulations that share common driver mutations but exhibit radically different biological properties. Phenotypic heterogeneity arises as a consequence of bidirectional interactions between cancer cells and the microenvironment that enable cells to switch in vivo from one phenotype to another (Hoek and Goding 2010; Hanahan 2022). The ability of cells to change phenotype underpins metastatic dissemination, contributes to both drug and immunotherapy tolerance, and represents a major challenge to effective anticancer therapy (Sharma et al. 2010; Kalkavan et al. 2022; Gerstberger et al. 2023). For example, in a wide range of cancer types, phenotype-specific expression and activation of the AXL receptor tyrosine kinase (RTK) have been linked to metastatic dissemination and therapy resistance (Asiedu et al. 2014; Wang et al. 2016; Gay et al. 2017; Boshuizen et al. 2018; Colavito 2020; Auyez et al. 2021; Shao et al. 2023).

Melanoma is a highly aggressive skin cancer that, unlike many cancer types, has well-defined phenotypic subtypes (Goodall et al. 2008; Hoek and Goding 2010; Rambow et al. 2018, 2019; Tsoi et al. 2018) that were initially characterized by the expression of the microphthalmia-associated transcription factor MITF, which controls

[6]**These authors contributed equally to this work.**
Corresponding authors: colin.goding@ludwig.ox.ac.uk, custodia.garcia@urjc.es

Article published online ahead of print. Article and publication date are online at http://www.genesdev.org/cgi/doi/10.1101/gad.351985.124. Freely available online through the *Genes & Development* Open Access option.

many aspects of melanoma biology (Goding and Arnheiter 2019). Consequently, melanoma represents an excellent model for understanding how cancer phenotype dictates disease progression and therapy resistance. Notably, whereas $MITF^{High}/AXL^{Low}$ cells can be proliferative, have poor metastatic potential, and are therapy-sensitive, $MITF^{Low}/AXL^{High}$ cells are slow-cycling, invasive, and refractive to therapy, including immune checkpoint inhibition (Konieczkowski et al. 2014; Müller et al. 2014; Rambow et al. 2018). Moreover, AXL activity has also been implicated in dormancy (Fane et al. 2022). However, although the AXL ligand GAS6 is expressed widely within tumors (Fane et al. 2022), how AXL activity might be preserved to maintain invasion and survival in metastasizing cells exiting the primary tumor or on entering vessels or how AXL is regulated to enable dormancy is not understood. One possibility is that the activation of key RTKs such as AXL is facilitated in migrating cells by microenvironmental factors other than their classical ligands. The nature of such activators is currently unknown, but their identification would provide a major insight into how the microenvironment might shape successful metastatic dissemination and therapy resistance.

One clue may come from evidence indicating that invasion, including that arising in response to inflammatory signaling, represents a survival strategy that evolved as a response to nutrient limitation (Falletta et al. 2017; García-Jiménez and Goding 2019). It therefore seems plausible that activation of the AXL RTK to promote survival of metastasizing cells could be linked to nutrient availability. In this respect, it has recently emerged that bidirectional interactions between cancer cells and adipocytes drive fatty acid uptake from the microenvironment and represent a major factor in disease progression and therapy resistance in a wide range of cancers (Zhang et al. 2018; Alicea et al. 2020; Ubellacker et al. 2020; Hoy et al. 2021; Altea-Manzano et al. 2023; Lumaquin-Yin et al. 2023; Demicco et al. 2024). For example, melanoma cells can come into contact with the adipocyte-rich dermis (Kwan et al. 2014), and adipocyte association with tumors is a marker of poor prognosis (Smolle et al. 1995). Moreover, oleic acid uptake from lymph can protect metastasizing melanoma cells from ferroptosis (Ubellacker et al. 2020), and FATP-dependent lipid uptake from aged fibroblasts can contribute to tolerance to BRAF inhibitor therapy (Alicea et al. 2020). However, although it is clear that fatty acid uptake from adipocytes (Hollander et al. 1986; Kwan et al. 2014; Lazar et al. 2016; Zhang et al. 2018; Lumaquin-Yin et al. 2023) and lymph (Ubellacker et al. 2020) plays a key role in melanoma progression, mechanistically how it rewires melanoma signaling to achieve its biological effects is poorly understood. It is also not known whether melanoma phenotype dictates the molecular response to certain fatty acids or whether the release of fatty acids from human adipocytes is a response to signals restricted to specific phenotypes.

Here we reveal that the capacity of melanoma cells to induce lipolysis in human adipose tissue is phenotype-specific and restricted to AXL^{High} cells, that oleic acid activates the AXL RTK to drive fatty acid uptake independent of FATPs, and that AXL activation by oleic acid promotes translocation of a caveolin–β-catenin complex essential for invasiveness and metastatic dissemination. The results highlight how a common microenvironmental nutrient shapes a phenotype-specific response associated with metastatic dissemination and therapy resistance.

Results

Induction of lipolysis in human adipose tissue by melanoma cells is restricted to undifferentiated $MITF^{Low}$-specific phenotypes

In vivo, metastasizing melanoma cells come into close proximity with adipocytes with the potential for bidirectional interactions, including cancer cell-induced adipocyte lipolysis and uptake of the released fatty acids by the cancer cells (Hollander et al. 1986; Kwan et al. 2014; Zhang et al. 2018; Lumaquin-Yin et al. 2023). However, whether human adipocytes release fatty acids in response to signals originating from specific phenotypic states is unknown. To investigate this, we used two *BRAF* mutant human melanoma cell lines, IGR37 and IGR39, that were derived from the same patient but were phenotypically very different: IGR37 cells express MITF but not AXL and represent a proliferative phenotype that is BRAF inhibitor (BRAFi)-sensitive. In contrast, IGR39 cells are $MITF^{Low}$, undifferentiated, invasive, and BRAFi-tolerant and express the AXL receptor tyrosine kinase, a hallmark of therapy resistance. The in vivo interaction between melanoma cells and adipocytes was recapitulated by coculture with human omentum adipose tissue explants separated by a membrane that permits exchange of small molecules, including lipids and exosomes, but does not allow passage of cells (Fig. 1A). Fatty acid uptake by the melanoma cells was then monitored using Nile red, a fluorescent lipophilic dye. Unexpectedly, only the undifferentiated $MITF^{Low}/AXL^{High}$ IGR39 cells, but not the $MITF^{High}/AXL^{Low}$ IGR37 cells, accumulated Nile red-stained lipid droplets (Fig. 1B). This result might have been obtained because only the IGR39 cells were competent to induce lipolysis in the human adipose tissue explants and/or because only IGR39 cells could take up the lipids released from the explants.

To distinguish between these possibilities, we initially examined the ability of both IGR39 and IGR37 cells to induce phosphorylation of hormone-stimulated lipase (HSL); phosphorylation activates HSL, which can hydrolyze stored triglycerides to free fatty acids, a key event in mobilization of adipose tissue fat stores. To ensure that the results were not limited to IGR37 and IGR39 cells, we used two additional melanoma cell lines: WM793 cells that, like IGR39, are $MITF^{Low}/AXL^{High}$ undifferentiated cells, and 501mel cells that, like IGR37, exhibit an $MITF^{High}$ proliferative phenotype. Human adipose tissue explants exposed to conditioned medium derived from the four melanoma cell lines for 4 days were examined for HSL phosphorylation status by Western blotting. The results (Fig. 1C) revealed that conditioned

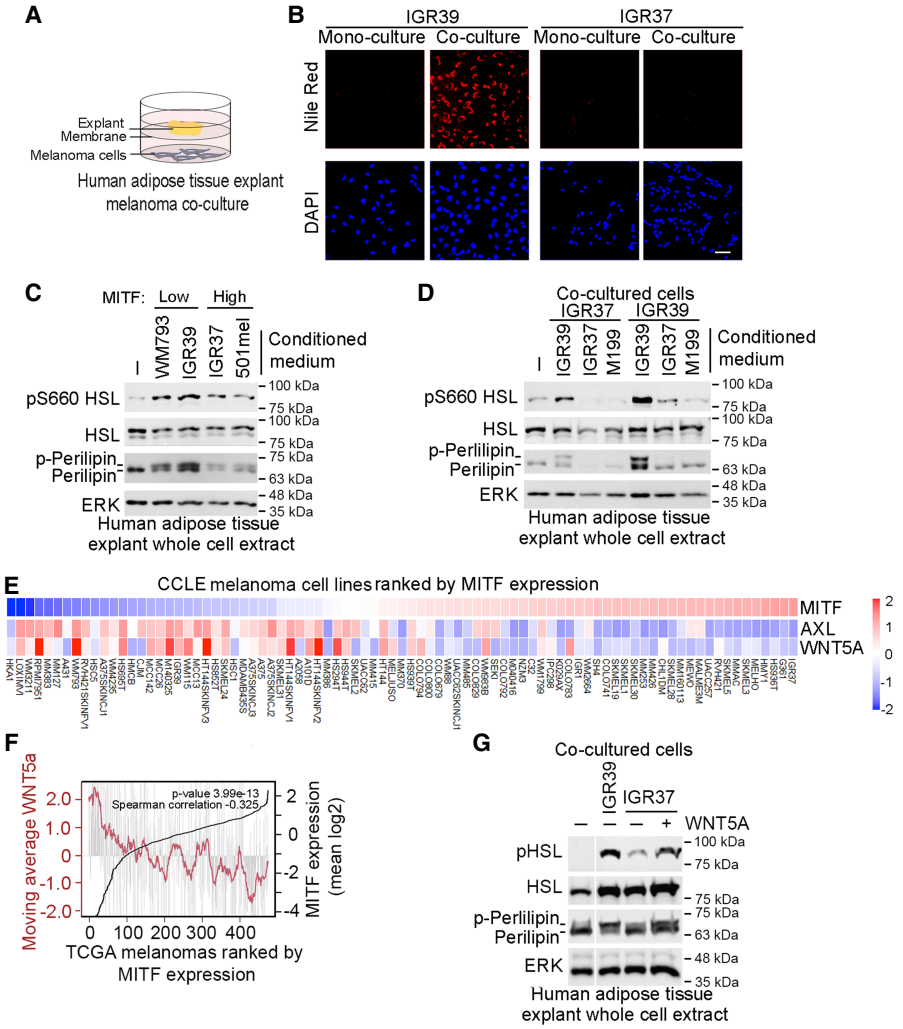

Figure 1. Only MITF^{Low} cells induce lipolysis in human adipose explants. (*A*) Schematic showing an experimental system for adipose tissue explant–melanoma cell coculture in which the explant and melanoma cells are separated by a 3 µm pore size lipid-permeable membrane. (*B*) Nile red staining of melanoma cells in monoculture or coculture with human adipose tissue explants for 4 days. DAPI was used to stain nuclei. Scale bar, 50 µm. (*C*,*D*) Western blots using the indicated antibodies of human adipose tissue explants cocultured with the indicated melanoma cells and exposed to the indicated conditioned medium for 4 days. (*E*) Heat map showing relative mRNA expression of the indicated genes in Cancer Cell Line Encyclopedia (CCLE) melanoma cell lines ranked by *MITF* expression. (*F*) Plot showing *WNT5a* mRNA expression (gray bars) in the Cancer Genome Atlas (TCGA) melanoma cohort ranked by *MITF* expression (black line). The moving average per 20 melanomas of *WNT5a* is shown as a maroon line. (*G*) Western blot of a human adipose tissue explant cocultured or not with the indicated cell lines with (+) or without (–) 50 ng of WNT5a. All samples were run on the same gel.

medium from both undifferentiated melanoma cell lines (WM793 and IGR39) induced phosphorylation of HSL, whereas conditioned medium from the MITF^{High} IGR37 and 501mel cells did not. In addition, conditioned medium from WM793 and IGR39 cells, but not that from IGR37 or 501mel cells, induced expression and phosphorylation of perilipin, a lipid droplet-associated protein and gatekeeper of lipolysis whose phosphorylation is a hallmark of adipocyte lipolysis (Greenberg et al. 1991). ERK was used as a loading control.

The presence of molecules secreted by melanoma cells that induce lipolysis in human fat explants was confirmed by exchanging the conditioned media. IGR37 or IGR39 cells were cocultured with human adipose tissue explants in conditioned medium from IGR39 cells or IGR37 cells or in M199 adipocyte culture medium as a control. The results (Fig. 1D) confirmed that the cocultured undifferentiated IGR39 cells could induce lipolysis, which was detected using antibodies for HSL and perilipin phosphorylation. However, when the medium was substituted with that from IGR37 cells or M199 medium, p-HSL and p-perilipin were reduced to baseline. Moreover, cocultured IGR37 cells could not induce markers of lipolysis in human adipose tissue explants unless conditioned medium from IGR39 cells was present. Collectively, these results indicate that factors secreted from the MITF^{Low}/

AXL^{High} undifferentiated melanoma cells were required to induce lipolysis in human adipose tissue explants.

To rule out any defects in uptake of free fatty acids by IGR37 cells, we next exposed IGR37 and IGR39 cells to oleic acid, an 18:1 long chain monounsaturated fatty acid, and examined the accumulation of lipid droplets. Oleic acid was used because it is the most abundant fatty acid in human adipose tissue (Insull and Bartsch 1967; Kokatnur et al. 1979; Hodson et al. 2008), and previous work has shown that uptake of oleic acid from lymph can enhance survival and suppress ferroptosis in metastasizing melanoma cells (Ubellacker et al. 2020). In these experiments, we used 100 μM oleic acid, a concentration fivefold lower than that used previously to suppress ferroptosis (Ubellacker et al. 2020) and similar to that found in plasma from nonhypertensive subjects (Davda et al. 1995). As expected, exposure of MITF^{High} or MITF^{Low} cell lines to oleic acid led to accumulation of lipid droplets, which was revealed by staining with Oil red O (Supplemental Fig. S1A).

These observations indicate that although IGR37 cells cannot induce lipolysis in human adipose tissue explants, they are nevertheless capable of importing free fatty acids. We therefore cocultured IGR37 and IGR39 cells separated by a porous membrane with murine 3T3-L1 adipocytes preloaded with fluorescent BODIPY-FL, which acts as a fatty acid mimetic and is transported by the same mechanisms as natural lipid (Supplemental Fig. S1B; Bai and Pagano 1997). Any uptake of BODIPY-FL by cocultured melanoma cells therefore reflects both its release from the adipocytes and an ability of the melanoma cells to import it. Unlike the result obtained with human adipose tissue explants, both IGR37 and IGR39 cells were able to induce BODIPY-FL release from the 3T3-L1 cells and its uptake (Supplemental Fig. S1C). Taken together, our results indicate that both MITF^{Low} and MITF^{High} cells can take up oleic acid, but whereas both induce lipid release and uptake from the murine 3T3-L1 adipocyte, only undifferentiated MITF^{Low}/AXL^{High} cells are competent to induce lipolysis from human adipose tissue explants and import the lipids released. One possible explanation for the different response to 3T3-L1 adipocytes versus human adipose tissue explants in these assays is that 3T3-L1 maintenance culture medium contains factors such as dexamethasone, which can promote lipolysis (Xu et al. 2009), and consequently no prolipolysis factor derived from melanoma cells is required to stimulate lipid release.

Collectively, these data suggest that a soluble factor secreted from MITF^{Low}/AXL^{High} but not MITF^{High}/AXL^{Low} melanoma cells is able to induce lipolysis and lipid release from human adipose tissue explants. Although a range of factors might be responsible, to date, no melanoma-secreted factor able to induce lipid release from adipocytes has been identified. Previous studies that reported that Wnt5a activates noncanonical WNT signaling to drive melanoma invasion (Weeraratna et al. 2002), metastatic dissemination, maintenance of dormancy (Fane et al. 2022), and BRAF inhibitor resistance (Anastas et al. 2014) suggest that WNT5a might be a potential candidate. In support, circulating WNT5a can promote a proinflammatory state in visceral adipose tissue (Catalán et al. 2014) and can drive adipocyte dedifferentiation associated with loss of lipid droplets (Zoico et al. 2016). Thus, we analyzed the panel of melanoma cell lines in the Cancer Cell Line Encyclopedia (CCLE), which revealed that WNT5a was primarily expressed in MITF^{Low}/AXL^{High} cell lines (including IGR39 and WM793 cells) (Fig. 1E). The results obtained in these cell lines were recapitulated in the Cancer Genome Atlas (TCGA) melanoma cohort in which *WNT5a* was expressed predominantly in MITF^{Low} tumors (Fig. 1F), consistent with both low MITF (Carreira et al. 2006; Chauhan et al. 2022) and high WNT5a (Weeraratna et al. 2002) being associated with invasiveness. We therefore tested the ability of WNT5a to induce lipolysis in human adipose tissue explants. The results (Fig. 1G) confirmed that both p-Perilipin and p-HSL were robustly induced by coculture with IGR39 cells or by addition of WNT5a to the coculture with IGR37 cells. These data are consistent with WNT5a secreted by MITF^{Low}, but not MITF^{High}, cells contributing to their ability to induce lipolysis in human adipose tissue.

Fatty acid uptake by MITF^{Low} melanoma cells is FATP-independent

The observation that only undifferentiated melanoma cells were competent to induce effective lipolysis from human adipose tissue explants led us to reassess how fatty acids are transferred into melanoma cells. Previous work has demonstrated that fatty acid uptake from adipocytes or aged fibroblasts into melanoma cells is mediated by FATPs, as determined by the sensitivity of fatty acid uptake to lipofermata (Zhang et al. 2018; Alicea et al. 2020), a small molecule that specifically blocks the ability of FATPs to import long chain fatty acids (Sandoval et al. 2010). However, whether FATPs are also required for fatty acid uptake by undifferentiated melanoma cells is unknown. We therefore exposed two MITF^{High}/AXL^{Low} (501mel and IGR37) and two MITF^{Low}/AXL^{High} (IGR39 and WM793) human melanoma cell lines to oleic acid in the presence or absence of lipofermata to monitor the accumulation of intracellular lipid droplets within the melanoma cells using Oil red O (Fig. 2A, quantified in B). In the absence of exogenously added oleic acid, some melanoma cells may contain a few small lipid droplets likely originating from fatty acids present in the fetal calf serum used in the culture medium. In contrast, addition of oleic acid led to a dramatic increase in lipid droplet formation in all cell lines, though the level of accumulation in the MITF^{Low} (IGR39 and WM793) cell lines was moderately reduced. As anticipated, lipofermata substantially reduced lipid droplet accumulation in the MITF^{High}/AXL^{Low} (501mel and IGR37) cell lines. Unexpectedly, lipofermata exhibited no effect on lipid droplet accumulation in the MITF^{Low}/AXL^{High} IGR39 and WM793 cells. This result suggested that MITF^{Low}/AXL^{High} undifferentiated melanoma cell lines use an alternative pathway to take up long chain fatty acids. We therefore examined the mRNA expression of a series of FATPs encoded by the *SLC27A* gene family in our in-house panel of

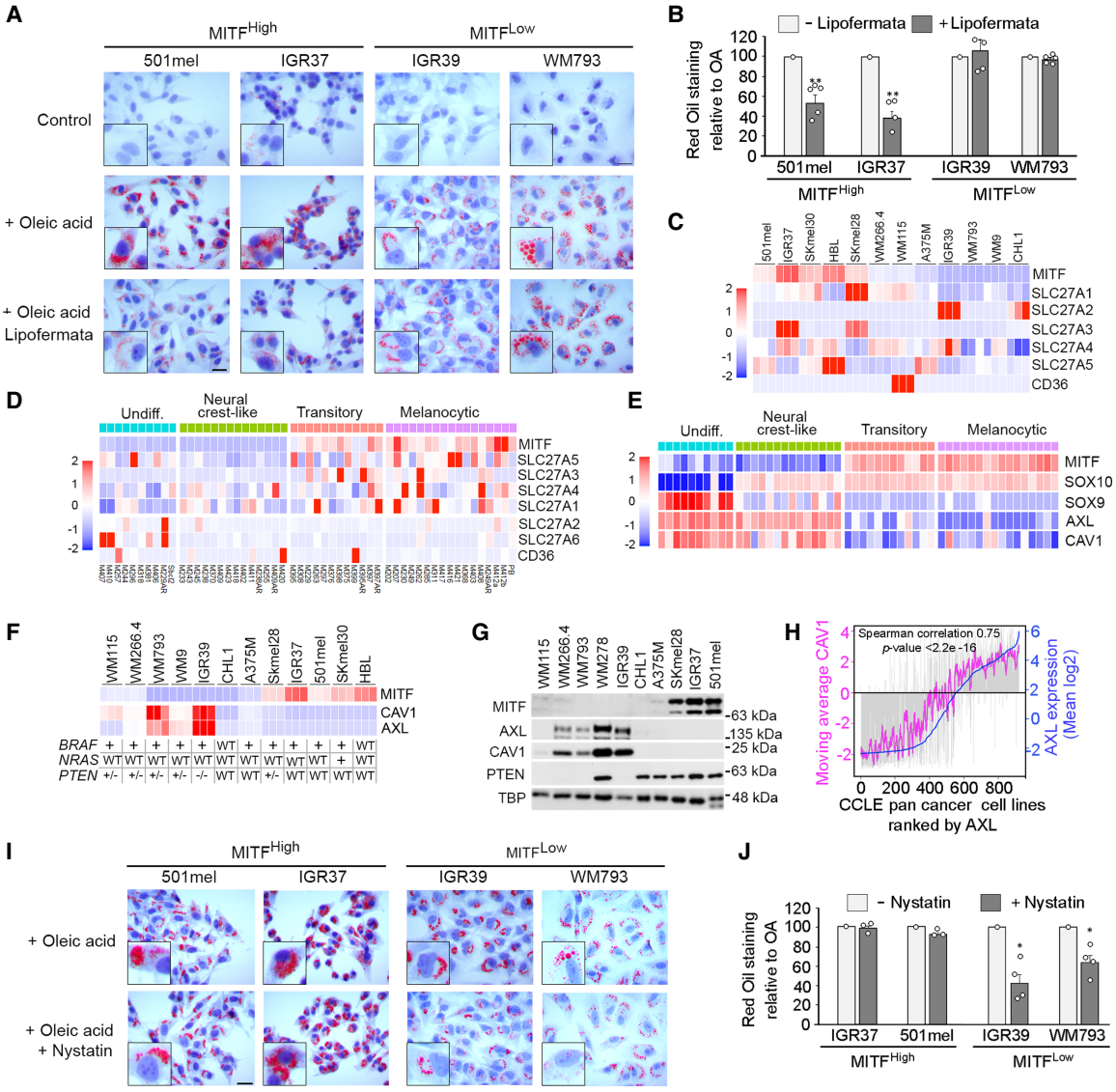

Figure 2. FATP-independent uptake of oleic acid by MITF^{Low} melanoma cells. (*A*) The indicated MITF^{High} and MITF^{Low} cell lines were exposed or not to 100 µM oleic acid for 16 h in the presence or absence of 1.25 µM lipofermata and stained using Oil red O. Scale bars, 50 µm. The *insets* show typical cells at higher magnification. (*B*) Quantification of Oil red O staining from the cells in *A*. $n = 3$ for IGR37; $n = 5$ for 501mel, IGR39, and WM793. Error bars indicate SEM. (**) $P < 0.01$; paired *t*-test. (*C*,*D*) Heat maps showing relative expression of MITF, CD36, and SLC27A family genes encoding FATPs in an in-house panel of 12 melanoma cell lines measured by triplicate RNA-seq (*C*) or in a panel of 53 melanoma cell lines clustered by phenotype as described by Tsoi et al. (2018) (*D*). (*E*) Heat map showing relative expression of *CAV1* in the Tsoi et al. (2018) cell lines using *MITF*, *SOX10*, *SOX9*, and *AXL* expression as markers of the indicated phenotypes. (*F*) Heat map showing expression of *MITF*, *AXL*, and *CAV1* mRNA in the indicated panel of 12 melanoma cell lines by RNA-seq in triplicate. The mutation status of *PTEN*, *BRAF*, and *NRAS* is indicated, where "+" indicates an activating mutation. (*G*) Western blot showing expression of the indicated proteins in a panel of 12 melanoma cell lines. (*H*) CCLE pan-cancer cell lines ranked by *AXL* expression, with the moving average of *CAV1* expression indicated in magenta. Gray bars indicate *CAV1* expression in each cell line. (*I*) Oil red O staining of the indicated melanoma cell lines exposed to oleic acid for 16 h and pretreated or not with 25 µM nystatin. The *insets* show typical cells at higher magnification. Scale bar, 50 µm. (*J*) Quantification of Oil red O staining in *I*. $n = 3$ for 501mel and IGR37; $n = 4$ for IGR39 and WM793. Error bars indicate SEM. (*) $P < 0.05$; paired *t*-test.

12 melanoma cell lines. We also included *CD36*, a fatty acid translocase that is expressed on metastasis-initiating cells characterized by increased fatty acid metabolism in a number of cancers (Pascual et al. 2017), and compared its expression with that of *MITF*, a marker for the more proliferative/differentiated cells. Remarkably, each cell line expressed a different pattern of FATP or *CD36* mRNA expression (Fig. 2C). For example, *CD36* was only significantly expressed in one MITF^{Low} line (WM115), whereas *SLC27A2* encoding FATP2, previously implicated in lipid uptake from fibroblasts (Alicea et al. 2020), was found in only two MITF^{Low} cell lines: IGR39 and CHL. In contrast

SLC27A1 encoding FATP1, reported to mediate lipid uptake by melanoma cells from adipocytes in vivo (Zhang et al. 2018), was more widely expressed, though predominantly in proliferative phenotype ($MITF^{High}$) cell lines. Notably, one cell line (WM793) appeared to express little of any FATP or *CD36* mRNA, consistent with its lipofermata-independent lipid droplet accumulation.

To extend these observations, we next used a panel of 53 well-characterized melanoma cell lines that fall into four distinct phenotypes based on their gene expression profiles (Tsoi et al. 2018). The results (Fig. 2D) largely recapitulated those of our in-house cell lines, with the majority of the FATP genes being more highly expressed in the two $MITF^{High}$ transient or melanocytic melanoma phenotypes. In contrast, *SLC27A2* and *SLC27A6* were expressed in a few $MITF^{Low}$ cell lines primarily with the undifferentiated phenotype. Interestingly, *CD36* was expressed to high levels in only three lines. These results, together with the observations that lipofermata predominantly affected oleic uptake in $MITF^{High}$ lines, raised the possibility that long chain fatty acid uptake in $MITF^{Low}$ melanoma cells is largely FATP-independent.

One candidate mechanism for fatty acid uptake is via caveolae, cholesterol, and sphingolipid-rich lipid rafts containing the protein caveolin. Caveolae are important for fatty acid transport in a number of cell types, including adipocytes (Pohl et al. 2004, 2005; Ring et al. 2006; Mattern et al. 2009). Remarkably, using the same panel of 53 melanoma cell lines in which different phenotypes can be distinguished using *MITF*, *SOX10*, and *SOX9* as markers (Fig. 2E) revealed that significant expression of *CAV1* mRNA encoding caveolin 1, a key component of caveolae in plasma membranes (Conde-Perez et al. 2015), was largely restricted to the $MITF^{Low}$ undifferentiated and neural crest-like melanoma cell lines that also express *AXL*, a hallmark of melanoma invasion and therapy resistance (Konieczkowski et al. 2014; Müller et al. 2014). Similar results were obtained using our in-house panel of lines, where RNA-seq (Fig. 2F) and Western blotting (Fig. 2G) also confirmed that CAV1 expression was largely restricted to the $MITF^{Low}/AXL^{High}$ cell lines. Notably, the correlation between *AXL* and *CAV1* expression was not restricted to melanoma cells but was recapitulated across cancer types in the Cancer Cell Line Encyclopedia (Fig. 2H).

To assess the impact of inhibiting caveolae-dependent endocytosis on fatty acid uptake by melanoma cells, we treated cells with oleic acid and used nystatin, a sterol-binding compound that disassembles caveolae in the membrane. As anticipated, the uptake of oleic acid by the $MITF^{High}/AXL^{Low}$ (501mel and IGR37) cell lines was unaffected by nystatin (Fig. 2I,J). In contrast, the accumulation of lipid droplets was reduced by nystatin in both the $MITF^{Low}/AXL^{High}$ IGR39 and WM793 cells. Collectively, the results indicate that although FATPs are used by the lipofermata-sensitive $MITF^{High}$ melanoma cells, $MITF^{Low}/AXL^{High}$ cells may use alternative mechanisms to take up fatty acids, including via caveolae. The observation that undifferentiated melanoma cells use a FATP-independent mechanism for fatty acid uptake is important because blocking FATP activity has been proposed as a potential anticancer therapy.

Phenotype-specific nuclear translocation of caveolin–β-catenin in response to oleic acid

To examine the molecular consequences of oleic acid uptake, we focused on the undifferentiated $MITF^{Low}$ melanoma cells that can induce lipolysis in human adipose tissue explants and import oleic acid in a lipofermata-independent fashion. Because *CAV1* expression is largely restricted to $MITF^{Low}/AXL^{High}$ melanoma cells, we performed immunofluorescence to detect CAV1 in the IGR39 cell line used as a model for the BRAFi-resistant undifferentiated phenotype. Under control conditions, CAV1 was excluded from nuclei, using Lamin B as a marker for the nuclear periphery, and was found primarily in the cytoplasm or associated with the plasma membrane, as expected (Fig. 3A). In contrast, exposure to oleic acid (OA) led to increased CAV1 expression and a proportion of the protein exhibiting nuclear localization. No nuclear CAV1 was observed if cells were exposed to palmitic acid (PA), an abundant 16:0 saturated long chain fatty acid. The effect of oleic acid on CAV1 nuclear accumulation was confirmed by Western blotting of fractionated cell extracts (Fig. 3B) that showed that OA could induce elevated levels of cytoplasmic CAV1 as well as an increase in nuclear CAV1. Nuclear accumulation of a proportion of CAV1, as well as its interaction with the inner nuclear membrane protein emerin, has been noted previously (Sanna et al. 2007; Chrétien et al. 2008), though the trigger for nuclear localization of CAV1 and its consequences have not previously been deciphered.

CAV1 can interact with β-catenin (Conde-Perez et al. 2015), the main effector of WNT signaling (Clevers 2006). β-Catenin plays a key role in the melanocyte lineage by driving the genesis of melanoblasts in the neural crest (Sommer 2011), activating melanocyte stem cells (Rabbani et al. 2011), suppressing melanoma senescence (Delmas et al. 2007), and promoting melanoma proliferation (Widlund et al. 2002) and metastasis (Damsky et al. 2011). The cytoplasmic interaction between β-catenin and CAV1 is inhibited by PTEN, a suppressor of PI3K (Conde-Perez et al. 2015) that is mutated in undifferentiated IGR39 cells. Although nuclear accumulation of β-catenin and regulation of its target genes are promoted by glucose-driven β-catenin acetylation in other cell types (Chocarro-Calvo et al. 2013), the mechanism by which β-catenin translocates to the nucleus in melanoma is unknown. Because oleic acid promotes nuclear localization of CAV1 and because CAV1 can interact with β-catenin, we asked whether oleic acid could control CAV1–β-catenin interaction to mediate their nuclear translocation.

Significantly, 4 h after addition of oleic acid, β-catenin nuclear localization was increased in IGR39 cells by both immunofluorescence (Fig. 3C) and Western blotting of fractionated extracts, using GAPDH and TBP as markers of the cytoplasmic and nuclear fractions, respectively (Fig. 3D). The ability of oleic acid to promote nuclear

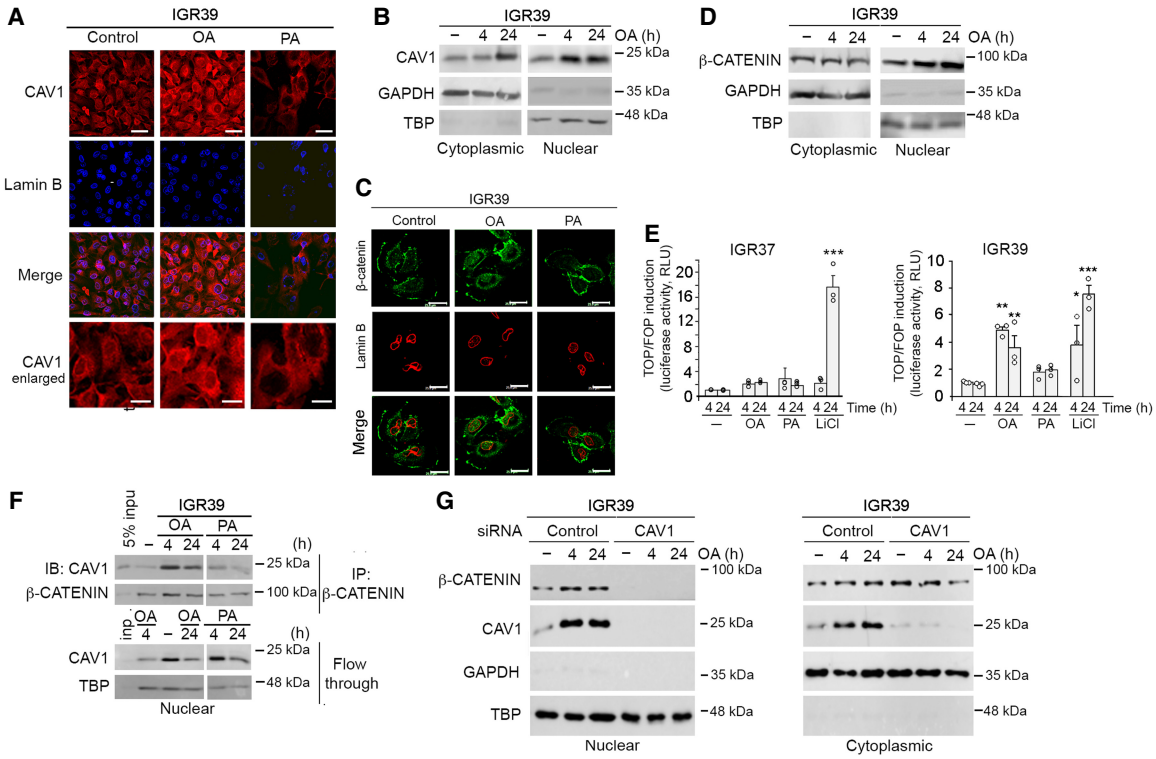

Figure 3. Oleic acid induces β-catenin–CAV1 interaction and nuclear localization. (*A*) Immunofluorescence of IGR39 cells using antibodies against the indicated proteins in cells exposed to 100 µM oleic (OA). Scale bars: *top* six panels, 50 µm; *bottom* three panels, 20 µm . (*B*) Western blots for the indicated proteins from fractionated IGR39 cells treated or not with 100 µM OA over time. GAPDH and TBP were used as markers of the cytoplasmic and nuclear fractions. (*C*) Immunofluorescence of IGR39 cells for the indicated proteins after exposure or not to 100 µM OA or palmitic acid (PA) for 6 h. Scale bars, 25 µm. (*D*) Western blot of fractionated IGR39 cells treated with oleic acid for the indicated times. (*E*) Luciferase reporter assays in the indicated cell lines showing the ratio of luciferase activity from the TOP:FOP-flash β-catenin activity reporters in melanoma cells exposed to 100 µM OA or PA for the indicated times. LiCl (10 mM) was used as a positive control. $N = 3$. Error bars indicate SEM. (*) $P < 0.05$, (**) $P < 0.01$, (***) $P < 0.001$; one-way ANOVA statistical test. (*F*) Western blot for the indicated proteins immunoprecipitated from IGR39 nuclear extract using anti-β-catenin antibody from cells treated or not with 100 µM OA or PA for the indicated times. The blot shows both immunoprecipitation (IP) and flowthrough (FT). (*G*) Western blots for the indicated proteins from fractionated IGR39 cells treated or not with 100 µM OA for the indicated times and transfected with either control or CAV1-specific siRNA. (*Left*) Nuclear fraction. (*Right*) Cytoplasmic fraction.

localization of β-catenin in the MITF^{Low} IGR39 cell line was similar to that of LiCl (Supplemental Fig. S2A), which is known to prevent β-catenin degradation by inhibiting GSK3β. Significantly, in CAV1-negative IGR37 cells, oleic acid had no effect on β-catenin nuclear accumulation, whereas LiCl increased both β-catenin levels and nuclear location (Supplemental Fig. S2B). The results obtained using immunofluorescence of IGR37 cells were confirmed by Western blotting of fractionated cell extracts (Supplemental Fig. S2C). The ability of oleic acid to induce nuclear accumulation of β-catenin was also reproduced using linoleic acid, an 18:2 unsaturated long chain fatty acid (Supplemental Fig. S2D). Importantly, in IGR39 cells, LiCl inhibited GSK3β through phosphorylation on S9, but oleic acid did not (Supplemental Fig. S2E). The result indicates that the mechanism underlying nuclear localization of β-catenin in response to oleic acid was not mediated by inhibition of GSK3β. In addition, we did not detect any change in phosphorylation of Y279 or Y216 on GSK3α and GSK3β, respectively, which are targets of FAK/PYK2 (Gao et al. 2015). We also noted no significant change in β-catenin mRNA levels in response to oleic acid (Supplemental Fig. S2F).

To test whether the oleic acid-driven nuclear accumulation of β-catenin could induce gene expression, we assessed the effect of exposure of cells to oleic acid on the SuperTOP-flash reporter (Veeman et al. 2003) containing canonical β-catenin–LEF/TCF response elements compared with the nonresponsive mutant variant (SuperFOP-flash). Using the MITF^{High}/AXL^{Low} IGR37 cell line that does not induce fatty acid release from human adipocytes, we failed to see any significant effect of oleic acid on the SuperTOP-flash reporter at 4 or 24 h, whereas a robust activation of the reporter was noted 24 h after addition of LiCl, which was used as a positive control (Fig. 3E, left panel). In contrast, exposure of MITF^{Low}/AXL^{High} IGR39 cells to oleic acid for 4 h led to a fivefold transcriptional activation of the SuperTOP-flash reporter (Fig. 3E, right panel) compared with the nonresponsive mutant variant. In these cells, LiCl treatment at 24 h increased the β-catenin-responsive

SuperTOP-flash reporter by almost eightfold compared with the nonresponsive reporter. No significant effect on the SuperFOP-flash reporter was observed using palmitic acid in either cell line. Thus, the transcriptional response of cells to oleic acid was phenotype- and fatty acid-specific.

We next asked whether oleic acid could affect β-catenin nuclear accumulation via promoting an association with CAV1. Coimmunoprecipitation of nuclear extracts using an anti-β-catenin antibody revealed that oleic acid led to increased interaction between β-catenin and CAV1 in the nuclear fraction that was not reproduced by exposing cells to palmitic acid (Fig. 3F). Significantly, although oleic acid promoted elevated levels of both nuclear and cytoplasmic CAV1, CAV1-specific siRNA prevented nuclear accumulation of β-catenin (Fig. 3G). Collectively, these data suggest that oleic acid triggers increased expression of CAV1 and formation of a β-catenin–CAV1 complex, and that CAV1 is necessary for oleic acid-induced nuclear translocation and activity of β-catenin. Because CAV1 is only expressed in the $MITF^{Low}/AXL^{High}$ undifferentiated cells, these observations uncover both a phenotype-specific molecular response to oleic acid and a phenotype-specific mechanism to mediate β-catenin nuclear localization.

Increased nuclear CAV1 expression in melanomas in proximity to adipocytes

Previous work has established that adipocytes in the vicinity of melanomas exhibit a reduced size (Zhang et al. 2018). Given the increased CAV1 expression and nuclear localization in cultured melanomas cells exposed to oleic acid, we asked whether, in human tumors, melanoma cells in the proximity to adipocytes also exhibit elevated nuclear CAV1 expression. We therefore examined human tissue samples in which vertical growth of a primary melanoma extends downward from the epidermis through the dermis into subcutaneous tissue comprising primarily adipocytes (Clark level V). In all, four Clark V primary melanomas were examined with similar results, two examples of which we present in Figure 4. After sectioning and hematoxylin staining, the tumors were first assessed by a pathologist, and three regions of interest were identified in the sample presented in Figure 4A: region 1, which is the melanoma core; region 2, which contains melanoma cells close to adipocytes; and region 3, which contains fully differentiated adipocytes with no melanoma infiltration. Tissue sections were then subjected to immunofluorescence using antibodies specific for CAV1 (Fig. 4A, green) or perilipin (Fig. 4A, red), a marker of differentiated adipocytes. Note that the use of xylene during the paraffin-embedding process will extract lipids from stores in both adipocytes and melanoma cells. The results of the immunofluorescence assay revealed that in region 1, located in the main body of the melanoma, CAV1 was poorly expressed. In contrast, in region 2, closest to the adipocyte layer, melanoma cells were interspersed with periplipin-positive adipocytes, and CAV1 expression was strongly upregulated and largely nuclear. Region 3 is primarily comprised of large adipocytes with little if any melanoma cell infiltration. Adipocytes in the vicinity of the tumor (region 2) were generally smaller than those present in the tumor (region 3) with no melanoma cell infiltration, consistent with adipocytes in the vicinity of melanoma cells undergoing lipolysis. Similar results were obtained in a second Clark V melanoma derived from a different patient in which four regions were examined (Fig. 4B). In this sample, region 1, derived from the main body of the melanoma, again exhibited very low CAV1 staining; region 2 contained a majority of melanoma cells exhibiting increased CAV1 expression compared with region 1; region 3 contained melanoma cells that exhibited high nuclear CAV1 staining in the vicinity of small adipocytes; and region 4 contained primarily large adipocytes with no melanoma infiltration.

In addition to the primary human melanoma samples, we also used a mouse allograft model in which murine YUMM1.7 ($Braf^{V600E}$; $Cdkn2a^{-/-}$; $Pten^{-/-}$) melanoma cells (Meeth et al. 2016) tagged with mCherry were implanted intradermally into 8 week old C57BL/6J mice. The derived tumors were frozen, allowing visualization of lipid droplets using BODIPY, and stained with anti-CAV1 before confocal imaging. Like the human primary melanomas, the results (Supplemental Fig. S3A,B) were consistent with the data obtained from cell lines. First, mCherry-positive melanoma cells in the core of the tumor distant from adipocytes do not contain lipid droplets (Supplemental Fig. S3A), but BODIPY-stained lipid droplets were found in melanoma cells close to adipocytes or at the migratory front. Second, melanoma cells distant from adipocytes express very low levels of CAV1 (Supplemental Fig. S3B), but levels increase in melanoma cells close to adipocytes as well as those at the invasive front. However, unlike in human melanomas, where the level of nuclear CAV1 was very high in adipocyte-proximal melanoma cells, only a low proportion of the CAV1 expressed in the mouse tumors was nuclear. This is similar to the $MITF^{Low}$ cells in culture, where oleic acid increases CAV1 expression, but only a proportion of CAV1 is nuclear. Thus, the human primary melanomas that we have examined have a greater proportion of CAV1 in the nucleus than those in the mouse model or cell lines. Whether this is because of human versus mouse differences or, more likely, because the human melanomas have spent a longer time growing in close proximity to adipocytes than the YUMM1.7 cells in the mouse model is not clear. Nevertheless, the human melanomas and mouse model recapitulate the major findings based on the cultured melanoma cell lines.

Oleic acid-mediated activation of SRC promotes CAV1 and β-catenin nuclear localization

Transcriptional activity of β-catenin requires its phosphorylation by SRC at Y333 (Yang et al. 2011). Whether oleic acid could induce β-catenin phosphorylation through SRC activation in $MITF^{Low}/AXL^{High}$ IGR39 cells is unknown. To investigate this, cells were treated with oleic acid, and β-catenin phosphorylation was probed by

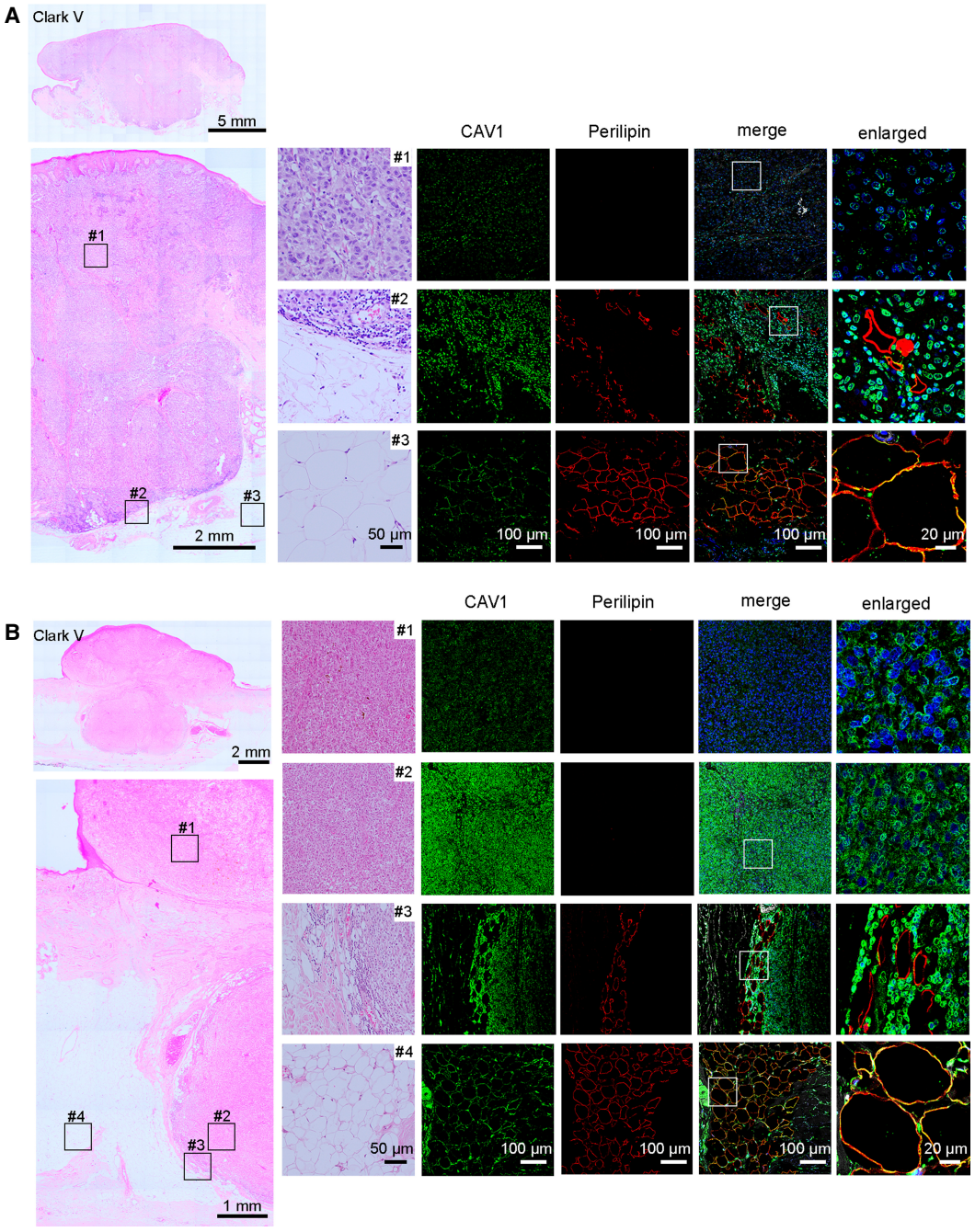

Figure 4. Elevated nuclear CAV1 in melanoma cells close to adipocytes in two Clark level V primary human melanomas. (*A*,*B*, *left* panels) Hematoxylin-stained sections through Clark level V melanomas. Scale bars: *A*, *top*), 5 mm; *A*, *bottom*, 2 mm; *B*, *top*), 2 mm; *B*, *bottom*, 1 mm. The *right* panels correspond to magnifications of areas of interest, which are indicated in *A* as *insets 1–3*, corresponding to the melanoma core (*1*), invasive front (*2*), and dermal adipocytes (*3*). In *B*, areas of interest are indicated by *insets 1–4*, corresponding to the melanoma core (*1*), melanoma cells close to adipocytes (*2*), invasive front (*3*), and dermal adipocytes (*4*). The first column of panels at the *right* corresponds to hematoxylin staining of the indicated *inset*. Scale bar, 50 µm. All additional panels at the *right* correspond to immunofluorescence using anti-CAV1 (green), anti-perilipin (red), and merge. Scale bars, 100 µm. The *top right* panels correspond to a more detailed view of the merged *inset* area. Scale bar, 20 µm.

Western blotting using a pY333 antibody. The results revealed that oleic acid induced robust phosphorylation of β-catenin at Y333 (Fig. 5A). We also noted that oleic acid increased CAV1 levels and induced phosphorylation of CAV1 at Y14 (Fig. 5B, top panels), a known SRC phosphorylation site (Li et al. 1996; Ortiz et al. 2016). No increase in CAV1 levels of phosphorylation was observed using palmitic acid (Fig. 5B, bottom panels), but linoleic acid could increase these levels (Supplemental Fig. S4A). These data suggest that oleic acid may induce activation of SRC in

IGR39 melanoma cells. Titration of oleic acid indicated a dose-dependent increase in CAV1 levels and phosphorylation (Fig. 5C) with 100 µM, similar to that in human plasma (Davda et al. 1995) being used for subsequent experiments. We next assessed the effect of oleic acid over time on phosphorylation of both CAV1 Y14 and SRC Y416, which is frequently used as a surrogate measure of SRC activity (Kmiecik et al. 1988) because pY416 stabilizes the SRC activation loop. The results (Fig. 5D) revealed that phosphorylation of CAV1 Y14 increases over time following exposure of cells to oleic acid, starting at 30 min. Similarly, within 30 min, oleic acid induces the activating Y416 phosphorylation of SRC, which is maintained over 24 h. We further confirmed that oleic acid mediates activation of SRC by examining phosphorylation of STAT3 Y705, another well-characterized SRC target (Cao

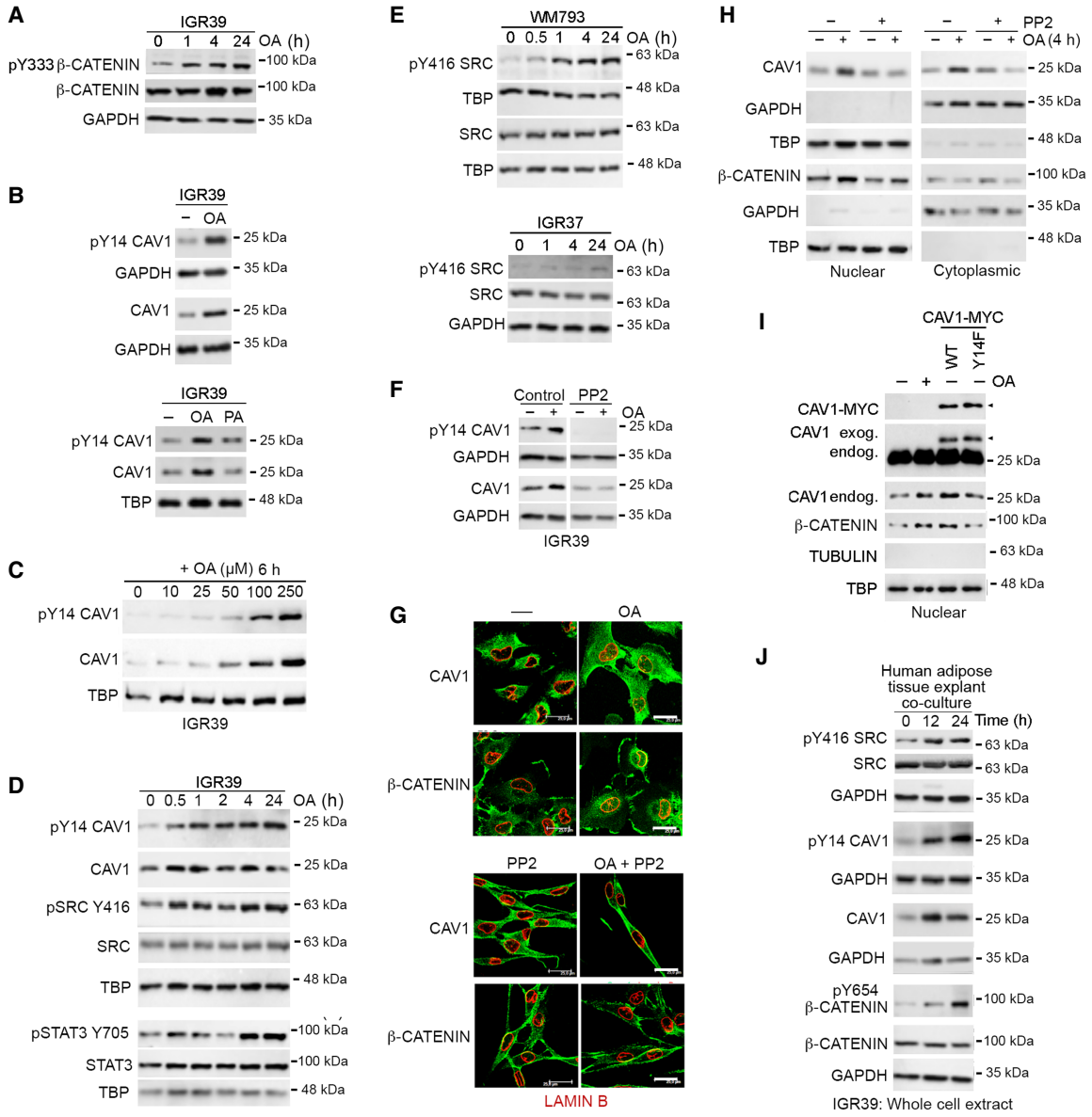

Figure 5. OA activates SRC in MITF^{Low} cells. (*A–E*) Western blots for the indicated proteins treated with 100 µM oleic acid (OA) or PA as indicated. (*F*) IGR39 cells were treated for 12 h with 10 µM PP2 with (+) or without (–) 100 µM OA for another 4 h before being analyzed by Western blot. Control samples were run on the same gel as PP2-treated samples. (*G*) Immunofluorescence for the indicated proteins in IGR39 cells pretreated for 12 h with 10 µM PP2 and then with (+) or without (–) 100 µM OA for a further 4 h. (*H*) Western blots of fractionated extract treated for 12 h with 10 µM PP2 with (+) or without (–) 100 µM OA for another 4 h. (*I*) Western blots for the indicated proteins of nuclear fraction from IGR39 cells treated with 100 µM OA and transfected where indicated with expression vectors for WT or Y14F mutant CAV1. Arrowheads indicate ectopic CAV1 WT or Y14F mutant. (*J*) Western blot for the indicated proteins of whole-cell extracts of IGR39 cells in coculture with adipose tissue explants for the indicated times. Adipose cells and IGR39 cells were separated by a 3 µm pore size membrane.

et al. 1996). The results (Fig. 5D, bottom panels) revealed that the increase in SRC Y416 over time induced by oleic acid was paralleled by elevated STAT3 Y705 phosphorylation. Significantly, the activation of SRC by oleic acid was reproduced in an alternative MITF^{Low}/AXL^{High} undifferentiated melanoma cell line, WM793 (Fig. 5E, top panels). In contrast, no SRC activation was detected in the MITF^{High}/AXL^{Low} line IGR37 (Fig. 5E, bottom panels). Moreover, like IGR39 cells, the WM793 line also exhibited increased phosphorylation of both SRC and CAV1 Y14 in response to oleic acid (Supplemental Fig. S4B). Consistent with SRC phosphorylating CAV1, treatment of IGR39 cells with the SRC family inhibitor PP2 (Fig. 5F) or depletion of SRC using siRNA (Supplemental Fig. S3C) abolished the phosphorylation of CAV1 at Y14 and reduced CAV1 levels.

The requirement of oleic acid-induced SRC activation for CAV1–β-catenin complex nuclear localization was tested by inhibition or depletion of SRC. Immunofluorescence revealed that inhibition of SRC family kinases using PP2 not only blocked the oleic acid-dependent increase in nuclear CAV1 but also prevented the nuclear localization of β-catenin (Fig. 5G). This result was confirmed using Western blotting (Fig. 5H), which showed that the oleic acid-induced nuclear accumulation of both CAV1 and β-catenin was blocked using PP2. The observations made using PP2 were confirmed using two SRC-specific siRNAs that prevented nuclear accumulation of both CAV1 and β-catenin (Supplemental Fig. S4D). Notably, ectopic expression of WT CAV1, but not a Y14F nonphosphorylatable mutant, was able to promote nuclear accumulation of β-catenin, mimicking the effect of oleic acid (Fig. 5I).

As these results were obtained using free oleic acid, we next ascertained whether the bidirectional interaction between melanoma cells and human adipose tissue explants could recapitulate the observations. The results revealed that exposure of IGR39 cells to human adipose tissue explants led, like oleic acid, to activation and phosphorylation of SRC and SRC-mediated phosphorylation of CAV1 Y14 and β-catenin Y654 (Fig. 5J).

Oleic acid activates an AXL–SRC axis

Taken together, the data so far reveal that (1) undifferentiated MITF^{Low}/AXL^{High} melanoma cells, but not MITF^{High}/AXL^{Low} cells, induce lipolysis in human adipose tissue explants; (2) FATP-independent fatty acid uptake by MITF^{Low} melanoma cells triggers activation of SRC, leading to the formation and nuclear translocation of a CAV1–β-catenin complex; and (3) even though both MITF^{High}/AXL^{Low} IGR37 and MITF^{Low}/AXL^{High} IGR39 cells can take up free oleic acid, SRC is only activated in MITF^{Low} IGR39 cells.

Because SRC can be activated by receptor tyrosine kinase (RTK)-mediated phosphorylation, we considered the possibility that oleic acid-induced SRC phosphorylation would be mediated through activation of an RTK whose expression is restricted to MITF^{Low} cells. One candidate was AXL, a key RTK whose expression has been associated with resistance to therapy in melanoma (Konieczkowski et al. 2014; Müller et al. 2014), breast, and other cancers (Auyez et al. 2021). Importantly, AXL is specifically expressed in most MITF^{Low} melanoma cells (Fig. 2E–G) and is normally activated by its ligand, GAS6, which promotes its dimerization. Instead, we considered the possibility that activation might also be facilitated via exposure of cells to oleic acid. We initially asked whether oleic acid would trigger autophosphorylation in *trans* of Y779, a marker of AXL activation. Western blotting of the MITF^{Low}/AXL^{High} WM793 melanoma cell line revealed that oleic acid induced elevated AXL Y779 phosphorylation, indicative of AXL activation, starting within 1 h of oleic acid addition (Fig. 6A).

Moreover, because MITF^{Low} cell lines that express CAV1 and AXL tend to be BRAF inhibitor (BRAFi)-resistant, we asked whether selection for increased BRAF inhibitor tolerance would lead to increased CAV1 and AXL expression. Significantly, selection of WM793 cells for increased resistance to BRAF inhibitors (Supplemental Fig. S5A) led to elevated expression of both AXL and CAV1, consistent with their expression in therapy-resistant cells (Supplemental Fig. S5B).

Activation of AXL by oleic acid was associated with elevated SRC phosphorylation (Fig. 6B) in both IGR39 and WM793 undifferentiated melanoma cells and was reproduced using LA (Supplemental Fig. S5C). Importantly, oleic acid-driven SRC phosphorylation was blocked by treatment with the AXL inhibitor ONO-7475 in both IGR39 and WM793 (Fig. 6C). Inhibition of AXL using ONO-7475 or a second inhibitor, R428 (bemcetinib), also prevented the induction of phosphorylation of CAV1 Y14 by oleic acid (Fig. 6D). Thus, oleic acid triggers a cascade of downstream events leading to nuclear localization of a CAV1–β-catenin complex (Fig. 6E).

Intriguingly, treatment of cells with the AXL inhibitor ONO-7475 or R428 decreased oleic acid uptake into both IGR39 and WM793 melanoma cells (Fig. 6F), as did inhibition of SRC with PP2 (Fig. 6G). This is consistent with oleic acid uptake in MITF^{Low} melanomas being mediated by caveolae (Fig. 2I,J) because CAV1 Y14 phosphorylation by SRC is necessary for caveola-mediated endocytosis (Hau et al. 2019). The results also reveal a potential positive feedback loop between oleic acid uptake and AXL activation.

We next investigated whether the ability of oleic acid to promote AXL activation and downstream SRC and CAV1 phosphorylation was permanent or reversible. The addition of oleic acid to IGR39 cells for 6 or 16 h led to the accumulation of lipid droplets that diminished over time after oleic acid removal (Fig. 6H). The 16 h treatment with oleic acid was used to help visualize the accumulation and subsequent loss of lipid droplets, which were barely visible after 6 h exposure of cells to oleic acid but exhibited a profile similar to that on treatment of cells with oleic acid for 16 h. Nevertheless, the addition of oleic acid for 6 h led to an initial activation of AXL and SRC and phosphorylation of CAV1 that was sustained for 24 h before being lost at 48 h after oleic acid removal

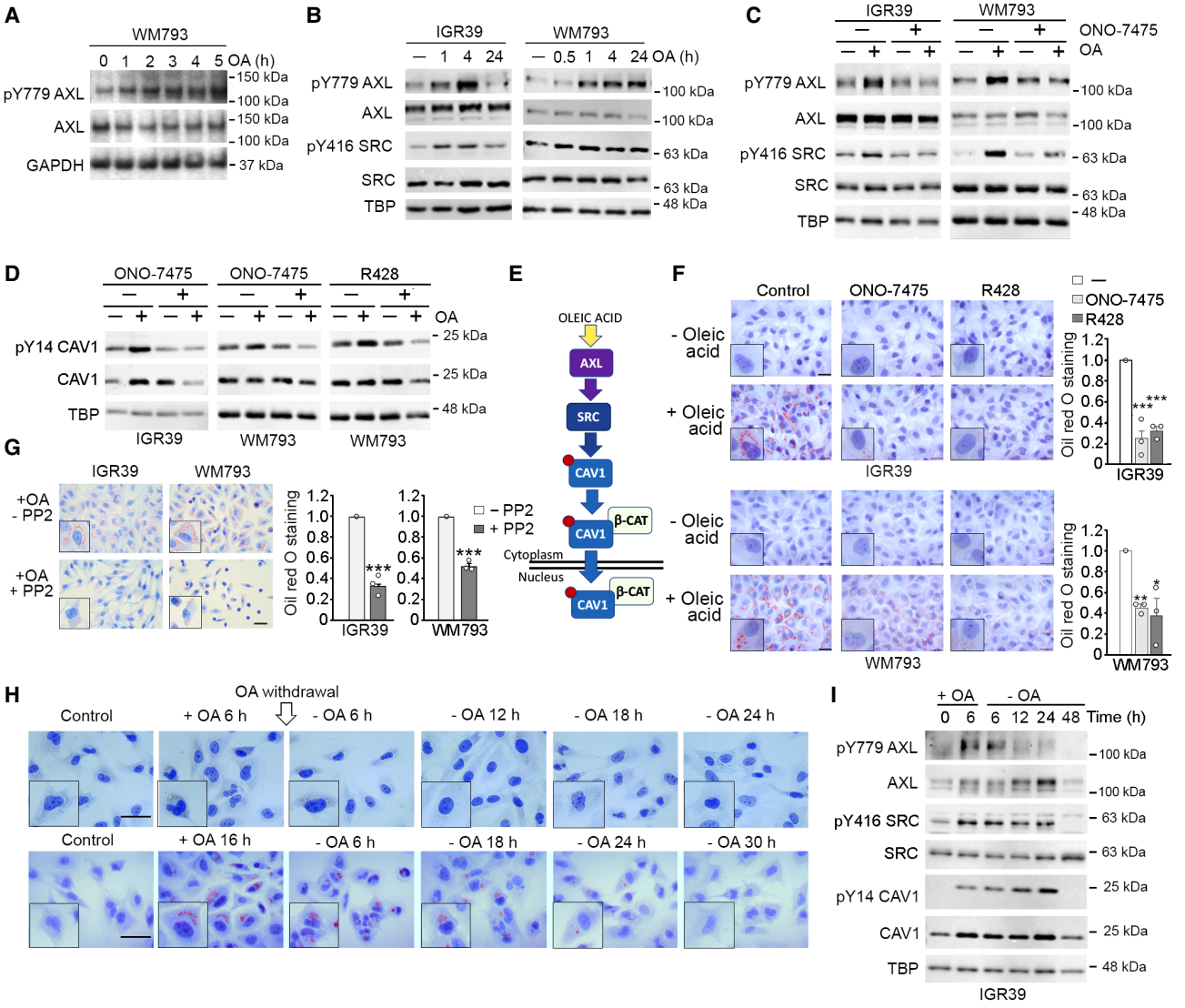

Figure 6. Oleic acid activates AXL. (*A–D*) Western blots of the indicated cell lines treated with 100 µM oleic acid for 4 h unless indicated otherwise and/or pretreated with AXL inhibitor ONO-7475 (0.5 µM for IGR39 or 0.1 µM for WM793) or R428 (0.5 µM) for 2 h prior to exposure to OA. (*E*) Schematic summarizing signaling downstream from oleic acid. (*F left*) Oil red O staining of IGR39 and WM793 cells exposed to AXL inhibitor ONO-7475 (0.5 µM) or R428 (0.5 µM) for 2 h with (+) or without (–) 100 µM OA for 12 h more. The *insets* show enlarged examples of typical cells. Scale bars, 50 µm. (*Right*) Quantification of Oil red O staining relative to OA alone. $N = 3$. Error bars indicate SEM. (*) $P < 0.05$, (**) $P < 0.01$, (***) $P < 0.001$; one-way ANOVA statistical test. (*G, left*) Oil red O staining of IGR39 and WM793 cells exposed or not to 100 µM oleic acid for 16 h in the presence or absence of 10 µM PP2. Scale bars, 50 µm. (*Right*) Quantification of Oil red O staining relative to OA alone. $N = 3$. Error bars indicate SEM. (***) $P < 0.001$; paired *t*-test. (*H*) Oil red O staining of IGR39 cells exposed to 100 µM OA for 6 h (*top* panels) or 16 h (*bottom* panels) before cells were washed with PBS followed by addition of fresh medium without OA. (*I*) Western blot of IGR39 cells exposed to OA and then placed in medium lacking OA for the indicated times.

(Fig. 6I). Thus, the effects of oleic acid are prolonged but reversible.

Oleic acid-mediated activation of AXL increases melanoma invasiveness

Because AXL and SRC activation can drive invasion, we assessed whether oleic acid could enhance invasion in IGR39 cells. The results obtained using a Matrigel *trans*-well assay revealed that oleic acid induced a robust increase in invasion in $MITF^{Low}/AXL^{High}$ IGR39 cells but not in $MITF^{High}/AXL^{Low}$ IGR37 cells (Fig. 7A). Similar results were obtained using human adipose tissue explants that in coculture induced invasion in IGR39 but not IGR37 cells (Fig. 7B). Invasion was induced in response to exposure to oleic acid and linoleic acid but not palmitic acid (Fig. 7C), consistent with oleic acid but not palmitic

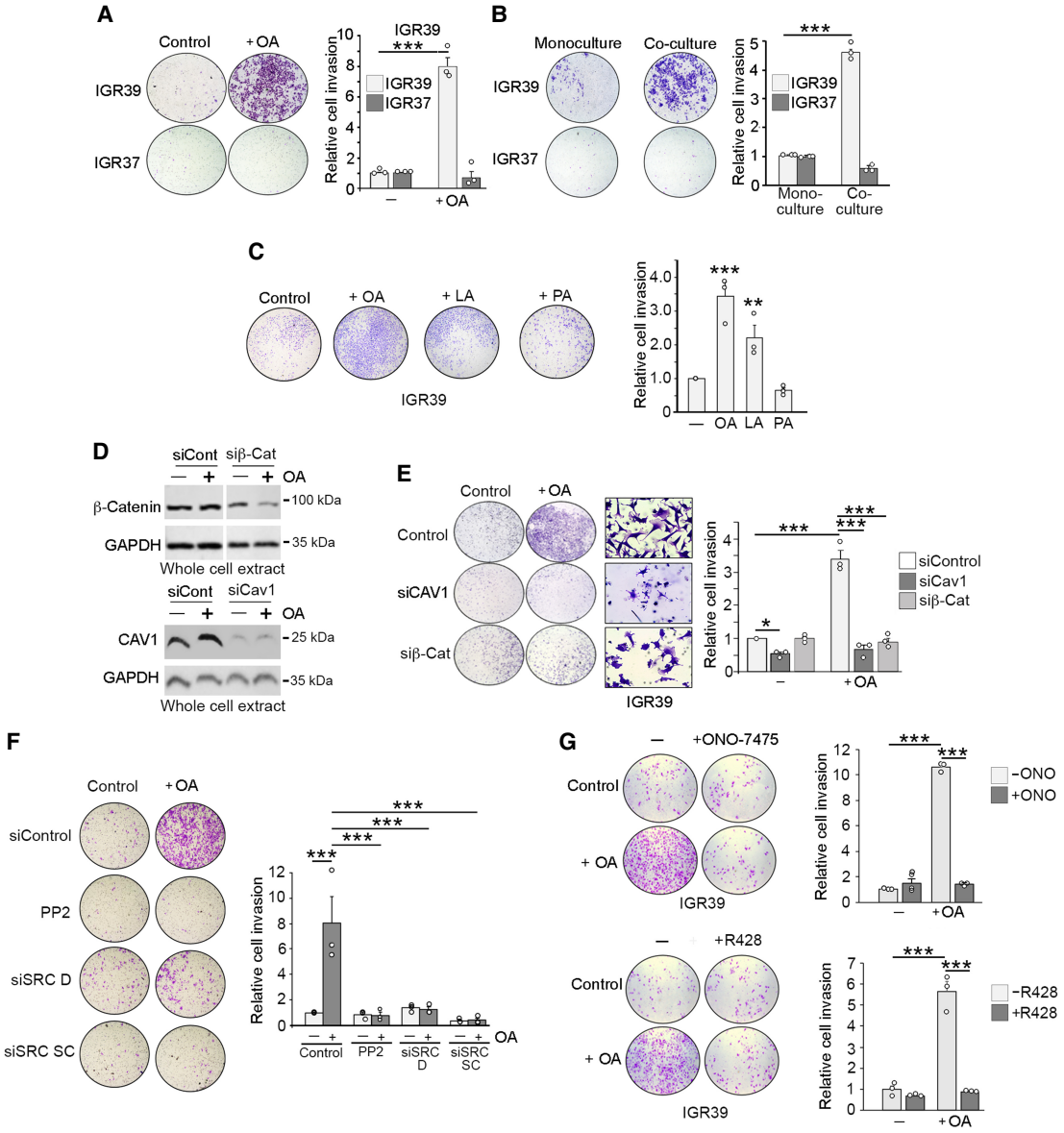

Figure 7. Oleic acid induces AXL-dependent invasion in melanoma. (*A–C*,*E–G*) Matrigel *trans*-well invasion assays showing invading cells stained with crystal violet. Where indicated, cells were treated with 100 µM oleic acid (OA), linoleic acid (LA), or palmitic acid (PA) and/or transfected with control or siRNAs targeting CAV1 or β-catenin (*E*) or SRC (*F*), cocultured with adipose tissue explants (*B*), or treated with SRC inhibitor PP2 (*F*) or AXL inhibitor ONO-7475 (0.5 µM) or R428 (0.5 µM) (*G*). Assays were performed for 22 h. Quantification is from $n = 3$ biological replicates, except for IGR39 in *A*, where $n = 4$. Error bars = SEM. (*) $P < 0.5$, (**) $P < 0.1$, (***) $P < 0.01$; one-way ANOVA statistical test. (*D*) Western blot of whole-cell extracts showing depletion of CAV1 or β-catenin after transfection with the indicated control or specific siRNAs. GAPDH was used as a loading control. Note that the β-catenin and GAPDH tracks in the *top* panels were run on the same gels.

acid being able to activate SRC and promote CAV1 phosphorylation (Fig. 5). siRNA-mediated depletion of either β-catenin (Fig. 7D, top panels) or CAV1 (Fig. 7D, bottom panels) inhibited oleic acid-induced invasion (Fig. 7E). Importantly, the oleic acid-mediated increase in invasiveness by IGR39 cells was also prevented by either SRC inhibition or siRNA-mediated SRC depletion (Fig. 7F) or using two different AXL inhibitors: ONO-75475 and R418 (Fig. 7G).

Discussion

It is now widely appreciated that tumors contain multiple phenotypically distinct populations of cancer cells that differ in their biological properties, some of which contribute to therapy resistance and metastatic dissemination, the two major obstacles to successful cancer treatment. However, whether specific phenotypic states might mediate unique bidirectional interactions with

the microenvironment is not well understood. Here we reveal a previously unsuspected ability of oleic acid, a widely available microenvironmental fatty acid, to facilitate activation of AXL, a phenotype-restricted receptor tyrosine kinase (RTK) implicated in melanoma dormancy and therapy resistance (Konieczkowski et al. 2014; Müller et al. 2014; Rambow et al. 2018; Fane et al. 2022). Oleic acid-driven activation of AXL leads to downstream SRC signaling that in turn promotes CAV1–β-catenin complex formation and nuclear localization, as well as the associated invasiveness that underpins metastatic dissemination. Importantly, our results obtained from cells in culture were strongly supported by our observations in human tumors, where CAV1 expression was increased and localized to the nucleus in melanoma cells in the vicinity of adipocytes in Clark level V primary melanomas. However, remarkably, the increase in nuclear CAV1 expression in melanoma cells close to adipocytes was not restricted to those melanoma cells immediately adjacent to adipose tissue. Instead, we observed a gradient of nuclear CAV1 expression extending for many cells distant from the adipose tissue. This suggests that melanoma-induced lipolysis in adipocytes may lead to effects of released fatty acids at a distance either by passing in between cells or, potentially more interestingly, by a process in which fatty acids taken up by one cell may subsequently be passed onto cells more distal from their source.

The observation that $MITF^{Low}/AXL^{High}$, but not $MITF^{High}/AXL^{Low}$, melanoma cells can induce lipolysis in and lipid uptake from human omentum adipose explants was unexpected. However, this is entirely in keeping with the hypothesis that $MITF^{Low}$ cells are invasive because they lack or fail to sense key nutrients that are needed to support high proliferation rates (García-Jiménez and Goding 2019). For example, as MITF activates transcription of the key fatty acid desaturase gene *SCD*, $MITF^{Low}$ cells express low levels of SCD and exhibit an increased saturated to monounsaturated fatty acid ratio, an imbalance that can stabilize an invasive state (Vivas-García et al. 2020). It makes sense, therefore, for invasive $MITF^{Low}$ cells to try to redress this imbalance by acquiring fatty acids from adipocytes. Indeed, the ability of melanoma cells, or cancer cells in general, to induce lipolysis in adipocytes through release of soluble factors may contribute to the loss of adipose tissue that is a characteristic of cancer-induced cachexia. However, although lipid release may be triggered by invasive $MITF^{Low}/AXL^{High}$ cells, it does not mean that they will revert to a proliferative state that would require not only both the carbon and energy provided by fatty acids but also nitrogen (amino acids) to fuel protein synthesis. Thus, lipolysis and fatty acid uptake may enable $MITF^{Low}/AXL^{High}$ cells to maintain their search for a niche suitable to promote proliferation. Note that we used the omentum as a source of adipose tissue partly because it is a known site for metastasis for many cancers, including melanoma. However, it is possible that adipose tissue from different anatomical sites might respond differently to signals derived from melanoma cells or release a different repertoire of lipids that may affect recipient melanoma cells in different ways.

Beyond activation of AXL, our results provide three additional and unanticipated insights. First, we show that only undifferentiated $MITF^{Low}$ melanoma cells, and not $MITF^{High}$ cells, are competent to induce lipolysis in human adipose tissue explants. Second, the mechanism of uptake of oleic acid by undifferentiated $MITF^{Low}/AXL^{High}$ melanoma cells is FATP-independent and therefore radically different from the lipofermata-dependent uptake operating in the differentiated $MITF^{High}$ phenotype. Third, our results reveal the molecular mechanism by which adipocytes or oleic acid promote (via activation of AXL and SRC) nuclear translocation of a CAV1–β-catenin complex in undifferentiated $MITF^{Low}$ melanoma cells. These observations have profound implications for our understanding of how bidirectional interactions with adipocytes in vivo may shape disease progression.

Previous studies associated AXL expression with an epithelial-to-mesenchymal (EMT) transition and invasiveness (Asiedu et al. 2014; Wang et al. 2016; Boshuizen et al. 2018; Shao et al. 2023). AXL expression is also linked to worse prognosis and resistance to therapies in a wide range of cancers, including prostate (Bansal et al. 2015), breast (Creedon et al. 2014), lung (Zhang et al. 2012), renal (Zhou et al. 2016), head and neck (Elkabets et al. 2015), and neuroblastoma (Debruyne et al. 2016). In melanoma, AXL is expressed in a high proportion of melanomas that have disseminated to lymph nodes (Sensi et al. 2011; Nyakas et al. 2022), and high expression of AXL is specifically associated with undifferentiated and invasive cellular phenotypes and is commonly linked to dormancy (Fane et al. 2022) and resistance to therapies (Konieczkowski et al. 2014; Müller et al. 2014; Rambow et al. 2018), including immune checkpoint inhibition (Hugo et al. 2016). Consequently, targeting AXL can eliminate specific subpopulations of melanoma cells and can cooperate with inhibition of the MAPK pathway (Boshuizen et al. 2018). In support, in preclinical models, targeting AXL can sensitize tumors to therapies (Auyez et al. 2021; Nyakas et al. 2022). This suggests that AXL activation is required to promote therapy resistance and to exert its prosurvival and prometastasis effects. However, although GAS6, the ligand of AXL, is widely expressed in tumors by cancer, stromal, and infiltrating immune cells (Auyez et al. 2021), how AXL might be activated in single metastasizing cells as they escape tumors and enter the lymphatic or blood vessels or invade other tissues where GAS6 may not be abundant was not understood. Our results address this key question by revealing how the availability of a key nutrient differentially impacts distinct melanoma cell phenotypes through activation of a phenotype-restricted RTK without addition of its ligand. How precisely oleic acid activates AXL remains unknown. One possibility is that oleic acid may increase membrane fluidity that would then facilitate AXL dimerization, which is necessary for its signaling. Importantly, oleic acid is the major circulating free fatty acid in tumor-associated lymph (Morfoisse et al. 2021), including in melanoma (Ubellacker et al. 2020), and can be released from adipocytes in proximity to melanoma cells (Zhang et al. 2018). Our observations therefore potentially have major

consequences for understanding disease progression in which oleic acid may promote increased invasion, survival, or dormancy by potentiating AXL activation.

Significantly, a recent study (Nyakas et al. 2022) suggested that the mechanism identified here using cell lines may reflect those operating within tumors: Proteomic analysis of tumors identified a reduction in β-catenin and CAV1 levels in AXL inhibitor-treated mice, as well as upregulation of ferroptosis. This is important because we show in vitro that AXL activation by oleic acid induces elevated β-catenin signaling and CAV1 expression and that AXL inhibition prevents uptake of oleic acid, which is a potent suppressor of ferroptosis.

Activation of SRC, a prosurvival signal triggered by integrin interactions with extracellular matrix, has been linked to BRAFi resistance in vivo (Hirata et al. 2015). Oleic acid induction of SRC via AXL, as reported here, may provide a degree of "adhesion mimicry" that would suppress cell death to promote therapy resistance in nonattached, metastasizing cancer cells. If so, AXL expression in therapy-resistant cells in various cancers could serve as a vital survival mechanism, especially in cancers prone to invading adipose tissue (Hoy et al. 2021) or the lymphatic system. In this respect, the ability of oleic acid to facilitate activation of a key RTK extends the importance of fatty acids well beyond the ability of some, such as palmitate (Altea-Manzano et al. 2023), to promote proliferation via fatty acid oxidation.

In addition to fatty acid uptake from lymph or through melanoma-induced lipolysis in adjacent adipocytes, the activation of AXL by oleic acid has implications for our understanding of the impact of obesity and diabetes on cancer progression, because both are known risk factors for many cancers including melanoma (García-Jiménez et al. 2016). Elevated plasma free fatty acid (FFA) levels in obesity (Henderson 2021) and diabetes (Clore et al. 2002) will increase the probability of activation of AXL and its downstream (SRC–CAV1–β-catenin) signaling in $MITF^{Low}/AXL^{High}$ melanoma cells, promoting their survival, invasiveness, metastatic dissemination, and therapy resistance, and may contribute to the worse survival outcomes among individuals with a high body mass index. Consistent with this, mice fed a high-fat diet exhibit increased melanoma progression associated with elevated CAV1 as well as pCAV1 (Pandey et al. 2012), and dietary oleic acid correlates with increased CD36-dependent SRC activity in cervical cancer (Yang et al. 2018).

Importantly, CAV1 is known to play a key role in melanoma progression in mouse models. For example, overexpression of CAV1 in murine B16 melanoma cells suppresses subcutaneous tumor growth while enhancing metastasis formation (Felicetti et al. 2009; Lobos-Gonzalez et al. 2013). However, formation of metastases in these studies was prevented by the presence of E-cadherin, which results in colocalization of CAV1, E-cadherin, and β-catenin at the cell surface. Phosphorylation of CAV1 at Y14 by SRC (Li et al. 1996), which we show here is promoted by activation of AXL by oleic acid, leads to not only stabilization of SRC–CAV1 complex formation but also recruitment of SRC to focal adhesions (Gottlieb-Abraham et al. 2013). Moreover, although not examined here, SRC-mediated phosphorylation of E-cadherin can also lead to decreased cell adhesion and increased E-cadherin internalization as well as reduced E-cadherin interaction with β-catenin (Liu et al. 2015). Oleic acid-mediated activation of SRC signaling will therefore likely engage a variety of prometastasis mechanisms that together will promote disease progression.

Why $MITF^{High}$ phenotype cells use FATPs to take up fatty acids while uptake in $MITF^{Low}/AXL^{High}$ cells is FATP-independent is unclear. As FATPs have been found in species from bacteria and yeast to humans (Doege and Stahl 2006), we might expect that all cells would use FATPs to transport fatty acids. One possible explanation for this phenotype-specific difference is that undifferentiated $MITF^{Low}/AXL^{High}$ cells tend to be slow-cycling and would have reduced demands for energy and for building blocks, which are required to generate membranes in daughter cells, compared with more rapidly dividing $MITF^{High}$ cells. It therefore is plausible that the need for long chain fatty acids (LCFAs) by slow-cycling $MITF^{Low}/AXL^{High}$ cells can be met by non-FATP-mediated transport, but in proliferative $MITF^{High}$ cells, the high demand for LCFAs requires transport by FATPs. This hypothesis would be consistent with the recent observation that the melanocytic state, which is associated with $MITF^{High}$-driven differentiation, is characterized by increased uptake of oleic acid and accumulation of lipid droplets (Lumaquin-Yin et al. 2023) and suggests that divergent uptake mechanisms are coupled to different lipid usage. Importantly, $MITF^{Low}/AXL^{High}$ cells use a FATP-independent mechanism, requiring AXL activity and likely downstream phosphorylation of caveolin, consistent with the recent revelation that CAV1 is associated with lipid droplets (Johns et al. 2025). The invasive melanoma cells take up fatty acids in a FATP-independent fashion, which has significant implications for the therapeutic use of FATP or CD36 inhibitors as an effective anticancer strategy (Pascual et al. 2017; Zhang et al. 2018; Alicea et al. 2020) because $MITF^{Low}/AXL^{High}$ cells would be resistant to such inhibitors, as they are to many other drugs including those targeting BRAF.

Finally, previous work has failed to identify a nuclear localization signal in β-catenin, meaning that its nuclear localization presumably arises through regulated interaction with cofactors. Here, we reveal that oleic acid activates a novel AXL-, SRC-, and CAV1-dependent mechanism that can promote nuclear localization of β-catenin independent of addition of WNT, the canonical trigger for β-catenin nuclear localization. Although previous work has shown cytoplasmic β-catenin–CAV1 interaction in the absence of PTEN (Conde-Perez et al. 2015), neither the ability of this complex to translocate to the nucleus nor its regulation by an oleic acid/AXL/SRC axis was known. Significantly, the ability of oleic acid to drive nuclear translocation of β-catenin is restricted to $MITF^{Low}/AXL^{High}$ melanoma cells, because only the neural crest-like and undifferentiated phenotypes express CAV1 and AXL, whose expression we found is highly correlated in melanoma cells as well as in other cancer types. Thus,

our results reveal a role of AXL in coordinating lipid uptake with SRC-dependent nuclear accumulation of β-catenin and increased invasiveness. This mechanism may underpin AXL's role in promoting invasiveness, survival, or dormancy in melanoma cells (Fane et al. 2022). However, as our results have been obtained using a limited number of melanoma cell lines, it remains to be seen whether the molecular mechanisms uncovered here will be generally applicable across melanoma or indeed in other cancer types. For example, PTEN protein expression can affect the interaction between CAV1 and β-catenin (Conde-Perez et al. 2015), and although the IGR39 and WM793 cells used here are PTEN-negative, another cell line in our in-house panel, WM278, expresses PTEN as well as AXL and CAV1. Whether the downstream effects of oleic acid on AXL signaling are affected by PTEN expression remains unknown.

In summary, we show here that the capacity to induce lipolysis and fatty acid release from human adipocytes, the mechanisms for fatty acid uptake, and the subsequent impact of fatty acids on SRC–CAV1 and β-catenin signaling are all phenotype-dependent events in melanoma cells, restricted to undifferentiated $MITF^{Low}/AXL^{High}$ phenotypes. These undifferentiated melanoma phenotypes are linked to increased invasiveness, metastatic dissemination, dormancy, and therapy resistance and represent a major obstacle for melanoma therapy. Here we reveal that FATP inhibitor-based therapies might not be sufficient to target these undifferentiated phenotypes, and that AXL/SRC/CAV1-dependent fatty acid uptake and signaling offer additional promising vulnerabilities. Our results therefore have major implications for our understanding of cancer progression and therapy resistance.

Materials and methods

Cell lines

All human melanoma cell lines were cultured in RPMI supplemented with 10% fetal bovine serum (FBS) plus 1% penicillin–streptomycin and maintained in a 5% CO_2 environment at 37°C. All cell lines were tested monthly for mycoplasma and were negative and were subjected to authentication by short tandem repeat (STR) profiling.

RNAi gene silencing

Cells plated in 6 well plates at 50% confluence were transfected with siRNA using JetPrime PolyPlus reagent (Genycell Biotech) following the manufacturer's instructions. After 2 days, cells were treated and collected to perform invasion assay or to be analyzed by Western blot. Specific siRNA oligonucleotides for β-catenin and control siRNA were obtained from Qiagen, Caveolin-1 and SRC siRNA were from Santa Cruz Biotechnology, and SRC siRNA were from Dharmacon, Inc.

Plasmid subcloning

Caveolin-1 WT or Y14F was subcloned from CAV1-mRFP plasmid (Tagawa et al. 2005) by PCR amplification with the indicated primers (Table 1) followed by a digestion with Bam HI and Xba I enzymes (New England Biolabs) for 2 h at 37°C. The fragments were gel-purified with a kit (Qiagen) and cloned into pcDNA3.1-myc-His plasmid (Promega). For sequencing, we used a sequence analyzer (ABI Prism 3100 Avant, Applied Biosystems). The correct introduction of the fragment was evaluated by plasmid sequencing using the BigDye cycle sequencing kit (Applied Biosystems).

Transient transfections

Cells were seeded in plates at 50% confluence and transfected using JetPei PolyPlus reagent (Genycell Biotech) following the manufacturer's instructions. After 36 h, cells were treated as indicated and collected for analysis by Western blot or immunofluorescence.

Whole-cell extracts

Cells were washed with iced PBS before extract preparation and scraped in RIPA buffer (10 mM Tris-HCl at pH 7.4, 5 mM EDTA, 5 mM EGTA, 1% Triton X-100, 10 mM $Na_4P_2O_7$ at pH 7.4, 10 mM NaF, 130 mM NaCl, 0.1% SDS, 0.5% Na-deoxycholate). After 5 min on ice, cells were pelleted at 12,000 rpm for 5 min at 4°C, and the supernatant was directly used as whole-cell extract or frozen at −80°C.

Fractionated cell extracts

After washing as before, cells were scraped in hypotonic buffer (20 mM HEPES at pH 8.0, 10 mM KCl, 0.15 mM EDTA, 0.15 mM EGTA, 0.05% NP40, protease inhibitors) and swollen for 10 min on ice before the addition of 1:2 vol of sucrose buffer (50 mM HEPES at pH 8.0, 0.25 mM EDTA, 10 mM KCl, 70% sucrose). Lysates were fractionated at 5000 rpm for 5 min at 4°C to obtain the cytoplasmic fraction in the supernatant. Nuclear pellets were further washed twice with washing buffer (20 mM HEPES at pH 8.0, 50 mM NaCl, $MgCl_2$ 1.5 mM, 0.25 mM EDTA, 0.15 mM EGTA, 25% glycerol, protease inhibitors), pelleted at 5000 rpm for 5 min at 4°C, and resuspended in nuclear extraction buffer (20 mM HEPES at pH 8.0, 450 mM NaCl, $MgCl_2$ 1.5 mM, 0.25 mM EDTA, 0.15 mM EGTA, 0.05% NP40, 25% glycerol, protease inhibitors) before centrifugation at 12,000 rpm for 5 min at 4°C to pellet and discard cell debris. The supernatants were used as nuclear fractions.

Immunoprecipitation

Whole-cell extracts were obtained in the same buffer without 0.1% SDS and 0.5% Na-deoxycholate. For immunoprecipitation from fractionated extracts, the hypotonic buffer was modified by adding 100 mM NaCl and 0.1% NP40. For immunocomplex formation, protein A/G-coated magnetic beads were washed three times with the

Table 1. *Reagents used in this study*

Reagents and software	Source	Identifier/reference	RRID
Antibodies			
Rabbit monoclonal anti-AXL (C89E7)	Cell Signaling Technology	8661	AB11217435
Rabbit polyclonal anti-phospho-Axl (Tyr779)	Cell Signaling Technology	96453	
Rabbit polyclonal anti-phospho-β-catenin (Y654)	Abcam	ab59430	AB_940822
Rabbit polyclonal anti-phospho-β-catenin (Y333)	Abcam	ab194797	
Mouse monoclonal anti-β-catenin	BD Transduction Laboratories	610154	AB_563467
Rabbit polyclonal anti-Caveolin-1	Cell Signaling Technology	3238	AB_2072166
Mouse monoclonal anti-Caveolin-1 antibody [7C8]	Abcam	ab17052	AB_443609
Rabbit polyclonal anti-phospho-Caveolin-1 (Tyr14)	Cell Signaling Technology	3251	AB_2244199
Rabbit polyclonal anti-phospho-Caveolin-1 (Tyr14)	BD Transduction Laboratories	611339	AB_398863
Rabbit polyclonal anti-ERK (C14)	Santa Cruz Biotechnology	SC-154	AB_2141292
Mouse monoclonal anti-GAPDH	Sigma Aldrich	G8795	AB_627679
Rabbit polyclonal anti-phospho-GSK-3β (Ser9)	Cell Signaling Technology	9336	AB_331405
Rabbit polyclonal anti-phospho-GSK3B (Tyr216, Tyr279)	Thermo Fisher Scientific	44604G	AB_2533691
Mouse monoclonal anti-GSK-3β	BD Transduction Laboratories	610201	AB_397600
Rabbit polyclonal anti-phospho-HSL (Ser660)	Cell Signaling Technology	45804	AB_2893315
Rabbit monoclonal anti-HSL (D6W5S) XP	Cell Signaling Technology	8381	AB_2798800
Rabbit polyclonal anti-Lamin B	Invitrogen	702972	AB_2784553
Mouse monoclonal anti-MITF	Abcam	ab12039	AB_298801
Mouse monoclonal anti-MYC tag	Cell Signaling Technology	2276	AB_331783
Rabbit monoclonal anti-Perilipin-1 (D1D8) XP	Cell Signaling Technology	9349	AB_10829911
Rabbit monoclonal anti-phospho-Src (Tyr416) (D49G4)	Cell Signaling Technology	6943	AB_10013641
Rabbit monoclonal anti-Src (36D10)	Cell Signaling Technology	2109	AB_2106059
Rabbit monoclonal anti-phospho-Stat3 (Tyr705; D3A7)	Cell Signaling Technology	9145	AB_2491009
Mouse monoclonal anti-STAT 3	Cell Signaling Technology	9139	AB_331757
Mouse monoclonal anti-α-Tubulin	Sigma	T5168	AB_477579
Rabbit polyclonal TFIID–TBP (N12)	Cell Signaling Technology	44059	AB_2799258
Chicken anti-mCherry	Novus Biologicals	NBP2-25158	
Donkey antichicken conjugated to rhodamine Red-X	Jackson ImmunoResearch	703-295-155	
Goat antirabbit IgG (H+L) HRPO	Bio-Rad	170-6515	AB_11125142
Goat antimouse IgG (H+L) HRPO	Bio-Rad	170-6516	AB_11125547
Rabbit antigoat IgG (H+L) HRPO	Bio-Rad	172-1034	AB_11125144

Continued

Table 1. *Continued*

Reagents and software	Source	Identifier/reference	RRID
Donkey antirabbit Alexa fluor 488	Invitrogen	A21206	AB_141708
Goat antimouse Alexa fluor 405	Abcam	ab175660	AB_2885184
Donkey antigoat Alexa fluor 647	Invitrogen	A21447	AB_2535864
Donkey antirabbit Alexa fluor 647	Invitrogen	A31573	AB_2536183
Bacterial and virus strains			
Subcloning efficiency DH5α bacteria	New England Biolabs	NEB5α	
Chemicals, peptides, and recombinant proteins			
RPMI 1640 media	Corning	5510-041-cv	
M199 medium	Lonza	BE12-117F	
Preadipocyte growth medium	Sigma	D5796	
IBMX	Sigma	I7018	
Insulin	Sigma	I5500	
L-glutamine (200 mM)	Lonza	BE17-605E	
Penicillin–streptomycin	Lonza	DE17-602E	
MEM NEAA	Gibco	11140-035	
Fetal bovine serum	Sigma	F7524	
Dexamethasome	Sigma	D5796	
Oleic acid	Sigma	O1383	
Palmitic acid	Sigma	P0500	
Lithium chloride	Sigma	L9650	
Lipofermata	Cayman Chemical	25869	
Nystatin	Deltaclon	S1934	
PP2	Deltaclon	S7008	
ONO-7475	Deltaclon	S8933	
R428 (Bencentinib)	Deltaclon	S2841	
Recombinant human/mouse Wnt-5a protein	R&D Systems	645-WN	
Bradford assay	Sigma	B6916	
BSA	Sigma	A7906	
Nile red	Sigma	N3013	
BODIPY 493/503	Thermo Fisher	D3922	
Oil red O	Sigma	O9755	
DAPI (4′,6-diamidino-2-fenilindol, dilactato)	Invitrogen	D3571	
Hoechst 33258	Life Technologies	H3569	
Mowiol 4-88	Sigma Aldrich	81381	
Protease inhibitor cocktail	Roche	04693132001	
JetPei PolyPlus reagent	Genycell Biotech	101-10N	
JetPrime PolyPlus reagent	Genycell Biotech	114-01	
Dynabeads protein A	Invitrogen	10002D	
Dynabeads protein G	Invitrogen	10004D	
High-density PET permeable support	Falcon	45353092	
Corning Matrigel invasion chamber	Corning	45354480	
Critical commercial assays			
Clarity ECL detection kit	Bio-Rad	170-5060	
RNA extraction RNeasy minikit QIAGEN	Qiagen	74106	
Dual-luciferase reporter assay system	Promega	E1960	
Pierce BCA protein assay kit	Thermo Fisher	23225	
Cell lines			
YUMM1.7	ATCC	Meeth et al. 2016	

Continued

Table 1. *Continued*

Reagents and software	Source	Identifier/reference	RRID
IGR39 (male) human melanoma cell line	Obtained from Luisa Lanfrancone	Aubert et al. 1980	CVCL_2076
IGR37 (male) human melanoma cell line	Obtained from Luisa Lanfrancone	Aubert et al. 1980	CVCL_2075
501mel (female) human melanoma cell line	Obtained from Ruth Halaban, Yale	Zakut et al. 1993	CVCL_4633
SKmel28 (male) human melanoma cell line	ATCC	Fogh et al. 1977	CVCL_0526
WM278 (female) human melanoma cell line	Obtained from Meenhard Herlyn	Herlyn et al. 1985	CVCL_6473
WM115 (female) human melanoma cell line	Obtained from Meenhard Herlyn	Herlyn et al. 1985	CVCL_0040
WM226.4 (female) human melanoma cell line	Obtained from Meenhard Herlyn	Herlyn et al. 1985	CVCL_2765
WM793 (male) human melanoma cell line	Obtained from Meenhard Herlyn	Herlyn et al. 1985	CVCL_8787
CHL-1 (female) human melanoma cell line	Obtained from Meenhard Herlyn		CVCL_1122
A375M (male) human melanoma cell line	ATCC	Giard et al. 1973; Fogh et al. 1977	CVCL_B222
3T3-L1 mouse fibroblast cell line	ATCC		CVCL_B222
Oligonucleotides			
Human *CTNNB1* RT qPCR primers F 5′–3′: GTGCTATCTGTCTGCTCTAGT R 5′–3′: CTTCCTGTTTAGTTGCAGCATC	Sigma	This study	
Human 18S RT qPCR primers F 5′–3′: AGTCCCTGCCCTTTGTACACA R 5′–3′: GCCTCACTAAACCATCCAATCG	Sigma Aldrich	This study	
siRNA human Caveolin-1	Santa Cruz Biotechnology	SC-29241	
SMARTpool: On-TargetPlus SRC siRNA	Dharmacon, Inc.	L-003175-00-0005	
siRNA β-catenin r(UCCAUUCUGGUGCCACCAC)d(TT) r(GUGGUGGCACCAGAAUGGA)d(TT)	Qiagen	This study	
Negative control siRNA	Qiagen	1027281	
Human Caveolin-1 subcloning primers F 5′–3′: CGCGGATCCGTGAACC GTCAGATCCGCTAG R 5′–3′: GCTCTAGAGCCTGCAA GTTGATGCGGACATTG	Sigma	This study	
Recombinant DNA			
Super8XTOPFlash	Obtained from R. Moon	Veeman et al. 2003	Addgene_12456
Super8XFOPflash	Obtained from R. Moon	Veeman et al. 2003	Addgene_12457
pcDNA3.1-Caveolin-1 WT-Myc-His	This study	N/A	
pcDNA3.1-Caveolin-1 Y14F-Myc-His	This study	N/A	
Software and algorithms			
LAS AF	Leica	SP5	SCR_013673
Glo-Max 96 multidetection system	Promega	N/A	
GraphPad Prism	GraphPad Software	https://www.graphpad.com	SCR_002798
ImageLab	Bio-Rad	ChemiDoc XRS+ System	SCR_014210
CXP	Becton-Dickinson	FACSCalibur	SCR_016722
ImageJ	N/A	https://imagej.nih.gov/ij/download.html	SCR_003070

Continued

Table 1. *Continued*

Reagents and software	Source	Identifier/reference	RRID
RNA-seq data	cBioPortal	http://www.cbioportal.org	SCR_014555
Molecular signatures	mSigDB	http://www.broadinstitute.org/msigdb	
Other			
TCGA analysis R script	N/A	Riesenberg et al. 2015	

extraction buffer before being coated with the primary antibody for 2 h at 4°C in a rotating wheel, followed by two washes with the same buffer to eliminates unbound antibody. Next, extracts were added overnight at 4°C in the rotating wheel. Immunocomplexes were washed twice and used for Western blotting.

Western blot

Protein lysates were subjected to 7.5% or 10% polyacrylamide SDS-PAGE. Proteins were transferred onto polyvinylidene difluoride membranes. Membranes were blocked with 5% nonfat milk or bovine serum albumin in TBS containing 0.1% Tween 20 and probed with the appropriate primary antibodies (see Table 1) overnight at 4°C. The specific bands were analyzed using ChemiDoc imaging systems (Bio-Rad).

Immunofluorescence microscopy

Cells in coverslips were washed three times, fixed with 4% paraformaldehyde in PBS (pH 7.4) for 10 min, washed again, permeabilized (PBS at pH 7.4, 0.5% Triton X-100, 0.2% BSA) for 5 min, blocked (PBS at pH 7.4, 0.05% Triton X-100, 5% BSA) for 1 h at room temperature, incubated with primary antibody overnight at 4°C, washed three times for 5 min, and incubated with the secondary antibody for 1 h at room temperature. For lipid staining after antibody incubation, cells were washed twice with PBS and stained with a solution containing 5 µg/mL BODIPY or Nile red. After 30 min incubation at room temperature, cells were washed twice with PBS. Slides were mounted, and images were acquired using an SP5 confocal microscope (Leica) with a 63× objective.

Luciferase reporter assay of TOP/FOP reporter luciferase activity

Melanoma cells seeded in 24 well plates at 50% confluence were cotransfected with 125 ng of the indicated promoter reporter and 25 ng of Renilla luciferase construct for normalization of transfection efficiency using JetPei Poly-Plus reagent (Genycell Biotech) following the manufacturer's instructions. Forty-eight hours after transfection, cells were treated with 100 µM oleic acid (OA) or 20 mM lithium chloride for another 4 or 24 h. Cells were lysed, and luciferase activity was measured in triplicate using the dual-luciferase reporter kit (Promega) and a Glo-Max 96 multidetector system (Promega). A minimum of three experiments was performed per cell line.

Crystal violet staining and cell density quantification

Thirty-thousand cells were plated in a 12 well plate and treated with DMSO and 100 µM oleic acid simultaneously over 5–7 days as indicated. The medium was replaced every 3 days. Plates were collected at time 0, 24, 72, 96, or 120 h; fixed with 4% PFA; and stained with 0.1% crystal violet for 15–30 min. Next, they were washed and dried. Crystal violet was resuspended in methanol, transferred to p96 plates, and analyzed by a Spectra Fluor (Tecan) at 570 nm. Viability was measured in duplicate in four independent experiments.

3T3-L1 coculture experiments

3T3-L1 cells (70,000 cells/well in a 12 well plate) were grown to 100% confluency in preadipocyte growth media (high-glucose DMEM [Sigma D5796], 10% newborn calf serum Sigma 12023C], 1% penicillin/streptomycin [Sigma P0781], 1% L-glutamine [Sigma G7513]). When cells reached confluence, the medium was changed, and 2 days later, differentiation was initiated. At day 0, differentiation medium with full induction cocktail was added (high-glucose DMEM [Sigma D5796], 10% FBS, 1% penicillin/streptomycin, 1% L-glutamine; induction cocktail: 0.5 mM IBMX [Sigma I7018], 1 µM dexamethasome [Sigma D1881], 5 µg/mL insulin [Sigma I5500]). At day 3, the medium was changed to differentiation media containing only 5 µg/mL insulin for 72 h. At day 6, once mature adipocytes were obtained, the medium was changed to simple differentiation media to preserve their adipocyte-differentiated state. Differentiated adipocytes were used for all coculture experiments.

For lipid transfer experiments, differentiated 3T3-L1 cells were preloaded with 1.5 µM BODIPY-FL-C16 in differentiation media (FBS + insulin) for 4 h and then washed twice using PBS + 0.1% BSA-free fatty acid. After 24 h, the preloaded adipocytes were washed again with PBS + 0.1% BSA-free fatty acid and placed in coculture with melanoma cells that had been seeded 24 h earlier in the *trans*-well chambers. The adipocytes were located at the bottom and the melanoma cells were at the top and maintained for 24 h in DMEM with 0.1% BSA-free fatty acid and without FBS. After 24 h in coculture, the melanoma cells were washed and fixed with 4% PFA. For picture acquisition,

the *trans*-well membranes were cut, stained with DAPI, and mounted under coverslips.

Adipose tissue and melanoma cell coculture experiments

Human adipose tissue samples were derived from surgical removal at Hospital Universitario Fundación Alcorcón (HUFA). Immediately after surgery, adipose tissue was placed into medium 199 (M199, Lonza) with 100 U/L penicillin, and 100 µg/mL streptomycin at room temperature. Blood vessels and connective tissue were removed, and uniform-sized tissue pieces of ~2 mm^3 were dissected.

Forty-eight hours before performing the coculture experiments, melanoma cells were seeded at 50% confluence in a 6 well plate, and adipose tissue pieces were cultured with melanoma cell medium. To perform fat–explant–melanoma coculture experiments, high-density PET-permeable supports with 3.0 µm pores were used (Falcon). The insert was placed in the 6 well plate where melanoma cells had previously been seeded, four to five pieces per well of adipose tissue were placed in the top, and 2 mL of medium of the indicated melanoma cell line was added. Forty-eight hours later, the fat and cells were collected, and changes in invasion capacity were analyzed by Western blot or immunofluorescence. To test whether lipolysis was induced by Wnt5a, melanoma IGR37 cells cocultured with adipose tissue were treated with 50 ng/mL Wnt5a for 4 days. Fat was collected and analyzed by Western blot.

Oil red O staining

Oil red O stock solution was prepared by dissolving 0.5 g of Oil red O (Sigma Aldrich) in 100 mL of isopropanol for 1 h at 56°C in a water bath. A working solution was prepared by mixing 30 mL of the Oil red O stock solution with 20 mL of distilled water, allowing it to stand for 10 min, and then filtering it. Cells in coverslips were washed three times, fixed with 4% paraformaldehyde in PBS (pH 7.4) for 10 min, briefly washed with running tap water, rinsed with 60% isopropanol, stained with freshly prepared Oil red O working solution for 15 min, and then rinsed with 60% isopropanol. Nuclei were stained with hematoxylin for 1 min and rinsed with distilled water. Slides were mounted, and images were acquired using a Zeiss optical microscope with a 40× objective. Oil red O intensity was quantified using ImageJ software. For each experiment, three different fields were evaluated per slide.

Matrigel invasion assays

Matrigel invasion assays were performed using invasion chambers from BD Biocoat (8 µm membrane inserts with Matrigel coating). Cells previously transfected and treated as indicated or cocultured with adipose tissue explants were cultured in medium without 0.2% FBS overnight and seeded at 100,000 cells per insert. Medium with 10% FBS was added to the bottom of the inserts. After 22 h of incubation, chambers were fixed in 3.7% paraformaldehyde for 2 min, washed in phosphate-buffered saline (PBS), stained with 1% crystal violet for 20 min, and washed in PBS. Cells remaining above the insert membrane were removed by gentle scraping with a sterile cotton swab. Slides were mounted, and images were acquired using a Zeiss optical microscope with a 5× objective. Cells were manually counted using ImageJ software. At least three biological replicates were performed.

RT-qPCR

Total RNA was isolated using the RNeasy minikit (Qiagen) or with Trizol (Invitrogen). cDNA was generated from 1 µg of RNA following the manufacturer's protocol. Reactions were performed in SYBR Green mix (Go-Taq, Promega) and analyzed using a 7500 Fast real-time PCR system (Applied Biosystems). Primers for human genes were designed using the Primer Blast application from NCBI (see Table 1). 18S ribosomal RNA and β-actin primers served as nonregulated controls. Relative expression was calculated using the *Ct* method, expressed as $2 - \Delta\Delta Ct$ (Livak and Schmittgen 2001). The PCR efficiency was ~100%.

Generation and analysis of mouse melanomas

YUMM1.7 cells were purchased from ATCC (Meeth et al. 2016), maintained as described by Meeth et al. (2016), and subcultivated using 0.25% (w/v) Trypsin-EDTA (Gibco 25200-056) at ratios that varied between 1:5 and 1:10. Cells were cultured at 37°C in 5% CO_2. YUMM1.7-Luciferase$^+$mCherry$^+$ melanoma cells were cultured under the same conditions as the parental cell line. The YUMM1.7 cells were infected with a lentivirus encoding for luciferase and mCherry expression (pCDH-EF1a-eFFly-mCherry cloned vector; a gift from Irmela Jeremias; plasmid 104833, Addgene) (Ebinger et al. 2016). Infected YUMM1.7-Luciferase$^+$mCherry$^+$ cells were sorted for mCherry expression using a BD FACS Aria fusion sorter (BD Biosciences). YUMM1.7-Luciferase$^+$mCherry$^+$ cells (2.5×10^5 cells) resuspended in 30 µL of Matrigel growth factor reduced basement membrane matrix (Corning 356231) were intradermally injected into 8 week old C57BL/6J mice obtained from the JAX repository. The grafted tumors were collected and fixed in 4% paraformaldehyde (PFA) for 24 h at 4°C with agitation. For cryopreservation, the samples were first incubated in 30% sucrose in 1× PBS for 48 h at 4°C in a rocking plate and then embedded in optimal cutting temperature compound (Sakura 4583). Frozen sections (16 µm) were cut from the tissue blocks using a Leica CM3050S cryostat (Leica Microsystems).

To label the lipid droplets, sections were washed with 1× TBS for 5 min and incubated with 1 µg/mL BODIPY 493/503 (Thermo Fisher 3922) for 20 min at room temperature. Samples were then washed three times with 1× TBS for 5 min and once with 1× PBS for 5 min. For nucleus detection, the sections were further incubated with DAPI (1:1000 in 1× PBS) for 15 min at room temperature, washed three times with 1× PBS for 5 min, and mounted in Mowiol 4-88 (Sigma Aldrich 81381).

For immunofluorescence, sections were washed with 1× PBS for 5 min and incubated with a blocking buffer

(5% horse serum, 0.8% Triton, 1% BSA in 1× PBS) for 1 h at room temperature, after which slides were incubated with the primary antibodies diluted in blocking buffer overnight at 4°C. Samples were washed three times with 1× PBS for 10 min before being incubated with the secondary antibodies and DAPI (1:1000) in blocking buffer for 1 h at room temperature. The sections were then washed three times with 1× PBS for 10 min and mounted in Mowiol 4-88. The primary antibodies used were rabbit anti-Caveolin-1 (1:400; Cell Signaling Technology 3238) and chicken anti-mCherry (1:800; Novus Biologicals NBP2-25158). The secondary antibodies used were donkey antirabbit conjugated to Alexa fluor 488 (1:400; Invitrogen A-21206) and donkey antichicken conjugated to rhodamine Red-X (1:400; Jackson ImmunoResearch 703-295-155). All labeled sections were imaged using an inverted LSM 980 confocal microscope (Carl Zeiss).

Analysis of human melanoma tissue samples

Melanoma patient samples were obtained from surgical resections of patients diagnosed with melanoma with a Clark level of V and a mean Breslow index of 10.32 mm. Samples and data from patients included in this study were provided by the Hospital La Paz Institute for Health Research Biobank (IdiPAZ Biobank [PT20-0004], integrated in the Biobanks and Biomodels ISCIII Platform) and processed following standard operating procedures with the appropriate approval of the Ethics and Scientific Committees, and by the Hospital Clínico San Carlos (C.I. 21/498-E, approved on June 25, 2021, C.I. 21/498-E). Fundamental ethical principles and rights promoted by Spain (LOPD 15/1999) and the European Union (2000/C364/01) were followed. Patient data were processed according to the Declaration of Helsinki (last revision 2013) and Spanish National Biomedical Research Law (14/2007, July 3).

Immunofluorescence was conducted using 5 µm sections of melanoma samples. Slides were deparaffinized by incubation for 10 min at 60°C and then incubated for 20 min at 95°C at pH 6.0 to detect perilipin and caveolin-1. Slides in slide holders were permeabilized (TBS at pH 7.4, 0.01% Triton X-100) for 15 min, incubated with anti-Perilipin (1:200 in TBS at pH 7.4, 0.01% Triton X-100, 1% BSA) for 2 h at room temperature, washed three times for 5 min in TBS, incubated with anti-caveolin-1 (1:200 in TBS at pH 7.4, 0.01% Triton X-100, 1% BSA) overnight at 4°C, and incubated with each secondary antibody (1:200 in TBS at pH 7.4, 0.01% Triton X-100, 1% BSA) for 2 h at room temperature. For detection of nuclei, slides were washed twice with PBS and stained with a solution containing 5 µg/mL DAPI for 15 min at room temperature. Slides were mounted, and images were acquired using a FV3000 confocal microscope (Olympus) with 4× and 20× objectives.

The primary antibodies used for immunofluorescence in tissues were anti-Caveolin-1 mouse monoclonal antibody (7C8; Abcam ab17052), rabbit polyclonal anti-Caveolin-1 (Cell Signaling Technology 3238), and rabbit monoclonal anti-Perilipin-1 (D1D8) XP (Cell Signaling Technology 9349). Secondary antibodies used were donkey antirabbit Alexa fluor 594 (Invitrogen R37119) and donkey antimouse Alexa fluor 647 (Invitrogen A31571).

Patient characteristics are indicated in Table 2.

Statistical analysis

Results are presented as fold induction (mean ± SEM) from at least three biological replicates. Comparisons between two independent groups were performed with Mann–Whitney *U*-tests. Tests for significance between two sample groups were performed with Student's *t*-test, and for tests for multiple comparisons were performed using ANOVA with Bonferroni's post-test.

RNA-seq

STR-authenticated (Eurofins genomic service), mycoplasma-free (Lonza LT07-318 and LT07-518) control melanoma cell lines were seeded in 6 well tissue-cultured dishes in RPMI 1640 (Gibco) supplemented with 10% FBS (Biosera) and 100 U/mL Pen Strep (Gibco) and maintained in a humidified chamber at 10% CO_2. Cells were collected at ~80% confluence, snap-frozen on dry ice, batched-processed using rNeasy minikit (Qiagen 74106) per the supplier's instructions, and eluted in 50 µL of nuclease-free water (Invitrogen 10977049). Samples with RIN values ≥9.5 (assessed using Agilent RNA 6000 nano kit; Agilent 5067-1511) were carried forward for library preparation using a QuantSeq forward kit (Lexogen 015.96) with 500 ng of input material and ERCC ExFold RNA spike-in mixes (Thermo Fisher 4456739). Sequencing was carried out on a HiSeq4000 (Illumina) by the Oxford Genomics Centre at the Wellcome Trust Centre for Human Genetics.

Bioinformatics

Raw fastq reads for the same samples sequenced across two lanes were stitched using UNIX, quality-controlled using fastqc (v0.11.9), and adaptor- and poly(A)-trimmed using Cutadapt. Processed fastq reads were mapped

Table 2. *Patient characteristics*

Patient characteristics	*N* (%)
Gender Male	4 (100%)
Age (median, years)	83
Breslow (median, mm)	10.32
Clark level	V
Clinical classification	
pT4	2 (50%)
pT4a	1 (25%)
pT4b	1 (25%)
Metastasis development	
Yes	1 (25%)
No	3 (75%)

against hg38 (GRCh38, 2015) + ERCC STAR index using rna-star (v2.5.1b) with quantMode enabled, allowing for soft clipping and splicing (minimum of 20 bp). Normalization and differential gene expression analyses were performed as described previously (Louphrasitthiphol et al. 2019, 2020; Vivas-García et al. 2020) using edgeR glmQLFTest. Heat maps were visualized using the R package pheatmap (v1.0.12).

Gene expression from 53 melanoma cell lines (Tsoi et al. 2018) was obtained from GSE80829 and the genes' classification as per the original study.

Gene expression data from the CCLE and TCGA were accessed through cBioPortal (Cerami et al. 2012; Gao et al. 2013). The moving average trend line of the bar plots in Figures 1F and 2H, representing the expression level of individual samples, was generated using a simple window size of 20. Spearman correlation and the significance were calculated using the cor.test function in R.

Material availability

All unique reagents generated in this study will be made available on request, but we may require a completed Materials Transfer Agreement.

Data availability

We declare that all data supporting the findings of this study are available within the article or from the corresponding author upon request. The RNA-seq data from the 12 in-house melanoma cell lines have been deposited in GEO (accession no. GSE184923; reviewer access token is yhcxcoicnnsflyl).

Ethics statement

Collection of human adipose tissue was performed according to the Institutional Review Board of HUFA act number 17/68 granting approval on June 8, 2017. Adipose tissue samples were collected using protocols approved by the corresponding Ethics Committees and following the legislation.

Melanoma samples and data from patients included in this study were provided by the IdiPAZ Biobank (PT20-0004, integrated in the Biobanks and Biomodels ISCIII Platform) and processed following standard operating procedures with the appropriate approval of the Ethics and Scientific Committees. All patients gave written informed consent for the use of their biological samples for research purposes. Fundamental ethical principles and rights promoted by Spain (LOPD 15/1999) and the European Union (EU; 2000/C364/01) were followed. All patients' data were processed according to the Declaration of Helsinki (last revision 2013) and Spanish National Biomedical Research Law (14/2007, July 3).

Mice were maintained in a certified animal facility in accordance with the European guidelines for laboratory animal use and care based on the 2010/63/EU Directive. All experiments involving mice were approved by the Animal Welfare and Ethics Body, Direção-Geral da Alimentação Veterinária, under protocol number 2022-08-09 013287.

Competing interest statement

The authors declare no competing interests.

Acknowledgments

We acknowledge for their collaboration the patients and the Hospital La Paz Institute for Health Research Biobank (IdiPAZ Biobank; PT20-0040, integrated into the Biobanks and Biomodel ISCII platform). Funding was provided by the Ludwig Institute for Cancer Research (to C.R.G, Y.V.-G., and P.L.), National Institutes of Health grants (PO1 CA128814-06A1 to Y.V.-G. and C.R.G., and R01 CA268597-01 to C.R.G. and P.L.), a European Union Marie Curie Training Fellowship (FP7-PEOPLE: PIEF-GA-2013-626098) and European Molecular Biology Organisation (EMBO) Long-Term Fellowship (ALTF 800–2013; to A.C.-C.), a Ministerio de Economía y Competitividad grant (SAF2016-79837-R to C.G.-J.), the Agencia Estatal de Investigación (MCIN/AEI/10.13039/501100011033; PID2019-104867RB-I00 and PID2023-151128OB-I00 to C.G.-J., and PID2021-127645OA-I00 to A.C.-C.), and Comunidad de Madrid (PEJ-2021-TL/BMD-21515 and PRECICOLON-CM-P2022/BMD-7212 to C.G.-J., and Ayudas Atracción de Talento 2017-T1/BMD-5334 and 2021-5A/BMD-20951 to A.C.-C.). A.S.-D. is supported by QuantOCancer Project Horizon European Union's Horizon 2020 program (grant 810653), and S.C.-M. is supported by Fundação para a Ciência e Tecnologia (2021.05801.BD). The project is also supported by a Fundação para a Ciência e Tecnologia grant to A.S.-D. (PTDC/MED-ONC/5553/2020). This research was funded in whole or in part by National Institutes of Health grants CA128814-06A1 and CA268597-01.

Author contributions: C.G.-J. and C.R.G. conceived the project and designed and interpreted experiments. A.C.-C., J.M.G.-M., M.J.-O., A.R.-S., Y.V.-G., S.C.-M., and P.L. performed experiments. J.C. and P.L. provided bioinformatic analysis. M.C.F. and M.D. provided fat explants. A.S.-D., C.G.-J., and C.R.G. provided resources, analysis, and supervision. C.G.-J. and C.R.G. wrote the manuscript.

References

Alicea GM, Rebecca VW, Goldman AR, Fane ME, Douglass SM, Behera R, Webster MR, Kugel CH III, Ecker BL, Caino MC, et al. 2020. Changes in aged fibroblast lipid metabolism induce age-dependent melanoma cell resistance to targeted therapy via the fatty acid transporter FATP2. *Cancer Discov* **10:** 1282–1295. doi:10.1158/2159-8290.CD-20-0329

Altea-Manzano P, Doglioni G, Liu Y, Cuadros AM, Nolan E, Fernández-Garcia J, Wu Q, Planque M, Laue KJ, Cidre-Aranaz F, et al. 2023. A palmitate-rich metastatic niche enables metastasis growth via p65 acetylation resulting in pro-metastatic

NF-κB signaling. *Nat Cancer* **4:** 344–364. doi:10.1038/s43018-023-00513-2

Anastas JN, Kulikauskas RM, Tamir T, Rizos H, Long GV, von Euw EM, Yang PT, Chen HW, Haydu L, Toroni RA, et al. 2014. WNT5A enhances resistance of melanoma cells to targeted BRAF inhibitors. *J Clin Invest* **124:** 2877–2890. doi:10.1172/JCI70156

Asiedu MK, Beauchamp-Perez FD, Ingle JN, Behrens MD, Radisky DC, Knutson KL. 2014. AXL induces epithelial-to-mesenchymal transition and regulates the function of breast cancer stem cells. *Oncogene* **33:** 1316–1324. doi:10.1038/onc.2013.57

Aubert C, Rouge F, Galindo JR. 1980. Tumorigenicity of human malignant melanocytes in nude mice in relation to their differentiation in vitro. *J Natl Cancer Inst* **64:** 1029–1040.

Auyez A, Sayan AE, Kriajevska M, Tulchinsky E. 2021. AXL receptor in cancer metastasis and drug resistance: when normal functions go askew. *Cancers (Basel)* **13:** 4864. doi:10.3390/cancers13194864

Bai J, Pagano RE. 1997. Measurement of spontaneous transfer and transbilayer movement of BODIPY-labeled lipids in lipid vesicles. *Biochemistry* **36:** 8840–8848. doi:10.1021/bi970145r

Bansal N, Mishra PJ, Stein M, DiPaola RS, Bertino JR. 2015. Axl receptor tyrosine kinase is up-regulated in metformin resistant prostate cancer cells. *Oncotarget* **6:** 15321–15331. doi:10.18632/oncotarget.4148

Boshuizen J, Koopman LA, Krijgsman O, Shahrabi A, van den Heuvel EG, Ligtenberg MA, Vredevoogd DW, Kemper K, Kuilman T, Song JY, et al. 2018. Cooperative targeting of melanoma heterogeneity with an AXL antibody–drug conjugate and BRAF/MEK inhibitors. *Nat Med* **24:** 203–212. doi:10.1038/nm.4472

Cao X, Tay A, Guy GR, Tan YH. 1996. Activation and association of Stat3 with Src in v-Src-transformed cell lines. *Mol Cell Biol* **16:** 1595–1603. doi:10.1128/MCB.16.4.1595

Carreira S, Goodall J, Denat L, Rodriguez M, Nuciforo P, Hoek KS, Testori A, Larue L, Goding CR. 2006. Mitf regulation of Dia1 controls melanoma proliferation and invasiveness. *Genes Dev* **20:** 3426–3439. doi:10.1101/gad.406406

Catalán V, Gómez-Ambrosi J, Rodríguez A, Pérez-Hernández AI, Gurbindo J, Ramírez B, Méndez-Giménez L, Rotellar F, Valentí V, Moncada R, et al. 2014. Activation of noncanonical Wnt signaling through WNT5A in visceral adipose tissue of obese subjects is related to inflammation. *J Clin Endocrinol Metab* **99:** E1407–E1417. doi:10.1210/jc.2014-1191

Cerami E, Gao J, Dogrusoz U, Gross BE, Sumer SO, Aksoy BA, Jacobsen A, Byrne CJ, Heuer ML, Larsson E, et al. 2012. The cBio cancer genomics portal: an open platform for exploring multidimensional cancer genomics data. *Cancer Discov* **2:** 401–404. doi:10.1158/2159-8290.CD-12-0095

Chauhan JS, Hölzel M, Lambert JP, Buffa FM, Goding CR. 2022. The MITF regulatory network in melanoma. *Pigment Cell Melanoma Res* **35:** 517–533. doi:10.1111/pcmr.13053

Chocarro-Calvo A, García-Martínez JM, Ardila-González S, De la Vieja A, Garcia-Jiménez C. 2013. Glucose-induced β-catenin acetylation enhances Wnt signaling in cancer. *Mol Cell* **49:** 474–486. doi:10.1016/j.molcel.2012.11.022

Chrétien A, Piront N, Delaive E, Demazy C, Ninane N, Toussaint O. 2008. Increased abundance of cytoplasmic and nuclear caveolin 1 in human diploid fibroblasts in H_2O_2-induced premature senescence and interplay with $p38\alpha^{MAPK}$. *FEBS Lett* **582:** 1685–1692. doi:10.1016/j.febslet.2008.04.026

Clevers H. 2006. Wnt/β-catenin signaling in development and disease. *Cell* **127:** 469–480. doi:10.1016/j.cell.2006.10.018

Clore JN, Allred J, White D, Li J, Stillman J. 2002. The role of plasma fatty acid composition in endogenous glucose production in patients with type 2 diabetes mellitus. *Metabolism* **51:** 1471–1477. doi:10.1053/meta.2002.35202

Colavito SA. 2020. AXL as a target in breast cancer therapy. *J Oncol* **2020:** 5291952. doi:10.1155/2020/5291952

Conde-Perez A, Gros G, Longvert C, Pedersen M, Petit V, Aktary Z, Viros A, Gesbert F, Delmas V, Rambow F, et al. 2015. A caveolin-dependent and PI3K/AKT-independent role of PTEN in β-catenin transcriptional activity. *Nat Commun* **6:** 8093. doi:10.1038/ncomms9093

Creedon H, Byron A, Main J, Hayward L, Klinowska T, Brunton VG. 2014. Exploring mechanisms of acquired resistance to HER2 (human epidermal growth factor receptor 2)-targeted therapies in breast cancer. *Biochem Soc Trans* **42:** 822–830. doi:10.1042/BST20140109

Damsky WE, Curley DP, Santhanakrishnan M, Rosenbaum LE, Platt JT, Gould Rothberg BE, Taketo MM, Dankort D, Rimm DL, McMahon M, et al. 2011. β-Catenin signaling controls metastasis in braf-activated pten-deficient melanomas. *Cancer Cell* **20:** 741–754. doi:10.1016/j.ccr.2011.10.030

Davda RK, Stepniakowski KT, Lu G, Ullian ME, Goodfriend TL, Egan BM. 1995. Oleic acid inhibits endothelial nitric oxide synthase by a protein kinase C-independent mechanism. *Hypertension* **26:** 764–770. doi:10.1161/01.hyp.26.5.764

Debruyne DN, Bhatnagar N, Sharma B, Luther W, Moore NF, Cheung NK, Gray NS, George RE. 2016. ALK inhibitor resistance in ALK^{F1174L}-driven neuroblastoma is associated with AXL activation and induction of EMT. *Oncogene* **35:** 3681–3691. doi:10.1038/onc.2015.434

Delmas V, Beermann F, Martinozzi S, Carreira S, Ackermann J, Kumasaka M, Denat L, Goodall J, Luciani F, Viros A, et al. 2007. β-Catenin induces immortalization of melanocytes by suppressing $p16^{INK4a}$ expression and cooperates with N-Ras in melanoma development. *Genes Dev* **21:** 2923–2935. doi:10.1101/gad.450107

Demicco M, Liu XZ, Leithner K, Fendt SM. 2024. Metabolic heterogeneity in cancer. *Nat Metab* **6:** 18–38. doi:10.1038/s42255-023-00963-z

Doege H, Stahl A. 2006. Protein-mediated fatty acid uptake: novel insights from in vivo models. *Physiology* **21:** 259–268. doi:10.1152/physiol.00014.2006

Ebinger S, Özdemir EZ, Ziegenhain C, Tiedt S, Castro Alves C, Grunert M, Dworzak M, Lutz C, Turati VA, Enver T, et al. 2016. Characterization of rare, dormant, and therapy-resistant cells in acute lymphoblastic leukemia. *Cancer Cell* **30:** 849–862. doi:10.1016/j.ccell.2016.11.002

Elkabets M, Pazarentzos E, Juric D, Sheng Q, Pelossof RA, Brook S, Benzaken AO, Rodon J, Morse N, Yan JJ, et al. 2015. AXL mediates resistance to PI3Kα inhibition by activating the EGFR/PKC/mTOR axis in head and neck and esophageal squamous cell carcinomas. *Cancer Cell* **27:** 533–546. doi:10.1016/j.ccell.2015.03.010

Falletta P, Sanchez-del-Campo L, Chauhan J, Effern M, Kenyon A, Kershaw CJ, Siddaway R, Lisle R, Freter R, Daniels M, et al. 2017. Translation reprogramming is an evolutionarily conserved driver of phenotypic plasticity and therapeutic resistance in melanoma. *Genes Dev* **31:** 18–33. doi:10.1101/gad.290940.116

Fane ME, Chhabra Y, Alicea GM, Maranto DA, Douglass SM, Webster MR, Rebecca VW, Marino GE, Almeida F, Ecker BL, et al. 2022. Stromal changes in the aged lung induce an emergence from melanoma dormancy. *Nature* **606:** 396–405. doi:10.1038/s41586-022-04774-2

Felicetti F, Parolini I, Bottero L, Fecchi K, Errico MC, Raggi C, Biffoni M, Spadaro F, Lisanti MP, Sargiacomo M, et al. 2009.

Caveolin-1 tumor-promoting role in human melanoma. *Int J Cancer* **125:** 1514–1522. doi:10.1002/ijc.24451

Fogh J, Fogh JM, Orfeo T. 1977. One hundred and twenty-seven cultured human tumor cell lines producing tumors in nude mice. *J Natl Cancer Inst* **59:** 221–226. doi:10.1093/jnci/59.1.221

Gao J, Aksoy BA, Dogrusoz U, Dresdner G, Gross B, Sumer SO, Sun Y, Jacobsen A, Sinha R, Larsson E, et al. 2013. Integrative analysis of complex cancer genomics and clinical profiles using the cBioPortal. *Sci Signal* **6:** pl1. doi:10.1126/scisignal.2004088

Gao C, Chen G, Kuan SF, Zhang DH, Schlaepfer DD, Hu J. 2015. FAK/PYK2 promotes the Wnt/β-catenin pathway and intestinal tumorigenesis by phosphorylating GSK3β. *eLife* **4:** e10072. doi:10.7554/eLife.10072

García-Jiménez C, Goding CR. 2019. Starvation and pseudo-starvation as drivers of cancer metastasis through translation reprogramming. *Cell Metab* **29:** 254–267. doi:10.1016/j.cmet.2018.11.018

García-Jiménez C, Gutiérrez-Salmerón M, Chocarro-Calvo A, García-Martinez JM, Castaño A, De la Vieja A. 2016. From obesity to diabetes and cancer: epidemiological links and role of therapies. *Brit J Cancer* **114:** 716–722. doi:10.1038/bjc.2016.37

Gay CM, Balaji K, Byers LA. 2017. Giving AXL the axe: targeting AXL in human malignancy. *Brit J Cancer* **116:** 415–423. doi:10.1038/bjc.2016.428

Gerstberger S, Jiang Q, Ganesh K. 2023. Metastasis. *Cell* **186:** 1564–1579. doi:10.1016/j.cell.2023.03.003

Giard DJ, Aaronson SA, Todaro GJ, Arnstein P, Kersey JH, Dosik H, Parks WP. 1973. In vitro cultivation of human tumors: establishment of cell lines derived from a series of solid tumors. *J Natl Cancer Inst* **51:** 1417–1423. doi:10.1093/jnci/51.5.1417

Goding CR, Arnheiter H. 2019. MITF—the first 25 years. *Genes Dev* **33:** 983–1007. doi:10.1101/gad.324657.119

Goodall J, Carreira S, Denat L, Kobi D, Davidson I, Nuciforo P, Sturm RA, Larue L, Goding CR. 2008. Brn-2 represses microphthalmia-associated transcription factor expression and marks a distinct subpopulation of microphthalmia-associated transcription factor-negative melanoma cells. *Cancer Res* **68:** 7788–7794. doi:10.1158/0008-5472.CAN-08-1053

Gottlieb-Abraham E, Shvartsman DE, Donaldson JC, Ehrlich M, Gutman O, Martin GS, Henis YI. 2013. Src-mediated Caveolin-1 phosphorylation affects the targeting of active Src to specific membrane sites. *Mol Biol Cell* **24:** 3881–3895. doi:10.1091/mbc.e13-03-0163

Greenberg AS, Egan JJ, Wek SA, Garty NB, Blanchette-Mackie EJ, Londos C. 1991. Perilipin, a major hormonally regulated adipocyte-specific phosphoprotein associated with the periphery of lipid storage droplets. *J Biol Chem* **266:** 11341–11346. doi:10.1016/S0021-9258(18)99168-4

Hanahan D. 2022. Hallmarks of cancer: new dimensions. *Cancer Discov* **12:** 31–46. doi:10.1158/2159-8290.CD-21-1059

Hau AM, Gupta S, Leivo MZ, Nakashima K, Macias J, Zhou W, Hodge A, Wulfkuhle J, Conkright B, Bhuvaneshwar K, et al. 2019. Dynamic regulation of Caveolin-1 phosphorylation and caveolae formation by mammalian target of rapamycin complex 2 in bladder cancer cells. *Am J Path* **189:** 1846–1862. doi:10.1016/j.ajpath.2019.05.010

Henderson GC. 2021. Plasma free fatty acid concentration as a modifiable risk factor for metabolic disease. *Nutrients* **13:** 2590. doi:10.3390/nu13082590

Herlyn M, Thurin J, Balaban G, Bennicelli JL, Herlyn D, Elder DE, Bondi E, Guerry D, Nowell P, Clark WH, et al. 1985. Characteristics of cultured human melanocytes isolated from different stages of tumor progression. *Cancer Res* **45:** 5670–5676.

Hirata E, Girotti MR, Viros A, Hooper S, Spencer-Dene B, Matsuda M, Larkin J, Marais R, Sahai E. 2015. Intravital imaging reveals how BRAF inhibition generates drug-tolerant microenvironments with high integrin β1/FAK signaling. *Cancer Cell* **27:** 574–588. doi:10.1016/j.ccell.2015.03.008

Hodson L, Skeaff CM, Fielding BA. 2008. Fatty acid composition of adipose tissue and blood in humans and its use as a biomarker of dietary intake. *Prog Lipid Res* **47:** 348–380. doi:10.1016/j.plipres.2008.03.003

Hoek K, Goding CR. 2010. Cancer stem cells versus phenotype switching in melanoma. *Pigment Cell Melanoma Res* **23:** 746–759. doi:10.1111/j.1755-148X.2010.00757.x

Hollander DM, Devereux DF, Taylor CG, Taylor DD. 1986. Demonstration of lipolytic activity from cultured human melanoma cells. *J Surg Res* **40:** 445–449. doi:10.1016/0022-4804(86)90213-1

Hoy AJ, Nagarajan SR, Butler LM. 2021. Tumour fatty acid metabolism in the context of therapy resistance and obesity. *Nat Rev Cancer* **21:** 753–766. doi:10.1038/s41568-021-00388-4

Hugo W, Zaretsky JM, Sun L, Song C, Moreno BH, Hu-Lieskovan S, Berent-Maoz B, Pang J, Chmielowski B, Cherry G, et al. 2016. Genomic and transcriptomic features of response to anti-PD-1 therapy in metastatic melanoma. *Cell* **165:** 35–44. doi:10.1016/j.cell.2016.02.065

Insull W Jr, Bartsch GE. 1967. Fatty acid composition of human adipose tissue related to age, sex, and race. *Am J Clin Nutr* **20:** 13–23. doi:10.1093/ajcn/20.1.13

Johns E, Ma Y, Louphrasitthiphol P, Perelta C MVH, Raymond JH, Molina H, Goding CR, White RM. 2025. The lipid droplet protein DHRS3 is a regulator of melanoma cell state. *Pigment Cell Melanoma Res* **38:** e13208. doi:10.1111/pcmr.13208

Kalkavan H, Chen MJ, Crawford JC, Quarato G, Fitzgerald P, Tait SWG, Goding CR, Green DR. 2022. Sublethal cytochrome c release generates drug-tolerant persister cells. *Cell* **185:** 3356–3374.e22. doi:10.1016/j.cell.2022.07.025

Kmiecik TE, Johnson PJ, Shalloway D. 1988. Regulation by the autophosphorylation site in overexpressed pp60$^{c\text{-}src}$. *Mol Cell Biol* **8:** 4541–4546. doi:10.1128/mcb.8.10.4541-4546.1988

Kokatnur MG, Oalmann MC, Johnson WD, Malcom GT, Strong JP. 1979. Fatty acid composition of human adipose tissue from two anatomical sites in a biracial community. *Am J Clin Nutr* **32:** 2198–2205. doi:10.1093/ajcn/32.11.2198

Konieczkowski DJ, Johannessen CM, Abudayyeh O, Kim JW, Cooper ZA, Piris A, Frederick DT, Barzily-Rokni M, Straussman R, Haq R, et al. 2014. A melanoma cell state distinction influences sensitivity to MAPK pathway inhibitors. *Cancer Discov* **4:** 816–827. doi:10.1158/2159-8290.CD-13-0424

Kwan HY, Fu X, Liu B, Chao X, Chan CL, Cao H, Su T, Tse AK, Fong WF, Yu Z-LL. 2014. Subcutaneous adipocytes promote melanoma cell growth by activating the Akt signaling pathway: role of palmitic acid. *J Biol Chem* **289:** 30525–30537. doi:10.1074/jbc.M114.593210

Lazar I, Clement E, Dauvillier S, Milhas D, Ducoux-Petit M, LeGonidec S, Moro C, Soldan V, Dalle S, Balor S, et al. 2016. Adipocyte exosomes promote melanoma aggressiveness through fatty acid oxidation: a novel mechanism linking obesity and cancer. *Cancer Res* **76:** 4051–4057. doi:10.1158/0008-5472.CAN-16-0651

Li S, Seitz R, Lisanti MP. 1996. Phosphorylation of caveolin by src tyrosine kinases. The α-isoform of caveolin is selectively

phosphorylated by v-Src in vivo. *J Biol Chem* **271:** 3863–3868. doi:10.1074/jbc.271.7.3863

Liu W, Kovacevic Z, Peng Z, Jin R, Wang P, Yue F, Zheng M, Huang ML, Jansson PJ, Richardson V, et al. 2015. The molecular effect of metastasis suppressors on Src signaling and tumorigenesis: new therapeutic targets. *Oncotarget* **6:** 35522–35541. doi:10.18632/oncotarget.5849

Livak KJ, Schmittgen TD. 2001. Analysis of relative gene expression data using real-time quantitative PCR and the $2^{-\Delta\Delta C(T)}$ method. *Methods* **25:** 402–408. doi:10.1006/meth.2001.1262

Lobos-Gonzalez L, Aguilar L, Diaz J, Diaz N, Urra H, Torres VA, Silva V, Fitzpatrick C, Lladser A, Hoek KS, et al. 2013. E-cadherin determines Caveolin-1 tumor suppression or metastasis enhancing function in melanoma cells. *Pigment Cell Melanoma Res* **26:** 555–570. doi:10.1111/pcmr.12085

Louphrasitthiphol P, Ledaki I, Chauhan J, Falletta P, Siddaway R, Buffa FM, Mole DR, Soga T, Goding CR. 2019. MITF controls the TCA cycle to modulate the melanoma hypoxia response. *Pigment Cell Melanoma Res* **32:** 792–808. doi:10.1111/pcmr.12802

Louphrasitthiphol P, Chauhan J, Goding CR. 2020. *ABCB5* is activated by MITF and β-catenin and is associated with melanoma differentiation. *Pigment Cell Melanoma Res* **33:** 112–118. doi:10.1111/pcmr.12830

Lumaquin-Yin D, Montal E, Johns E, Baggiolini A, Huang TH, Ma Y, LaPlante C, Suresh S, Studer L, White RM. 2023. Lipid droplets are a metabolic vulnerability in melanoma. *Nat Commun* **14:** 3192. doi:10.1038/s41467-023-38831-9

Mattern HM, Raikar LS, Hardin CD. 2009. The effect of Caveolin-1 (Cav-1) on fatty acid uptake and CD36 localization and lipotoxicity in vascular smooth muscle (VSM) cells. *Int J Physiol Pathophysiol Pharmacol* **1:** 1–14.

Meeth K, Wang JX, Micevic G, Damsky W, Bosenberg MW. 2016. The YUMM lines: a series of congenic mouse melanoma cell lines with defined genetic alterations. *Pigment Cell Melanoma Res* **29:** 590–597. doi:10.1111/pcmr.12498

Morfoisse F, De Toni F, Nigri J, Hosseini M, Zamora A, Tatin F, Pujol F, Sarry JE, Langin D, Lacazette E, et al. 2021. Coordinating effect of VEGFC and oleic acid participates to tumor lymphangiogenesis. *Cancers* **13:** 2851. doi:10.3390/cancers13122851

Müller J, Krijgsman O, Tsoi J, Robert L, Hugo W, Song C, Kong X, Possik PA, Cornelissen-Steijger PD, Foppen MH, et al. 2014. Low MITF/AXL ratio predicts early resistance to multiple targeted drugs in melanoma. *Nat Commun* **5:** 5712. doi:10.1038/ncomms6712

Nyakas M, Fleten KG, Haugen MH, Engedal N, Sveen C, Farstad IN, Florenes VA, Prasmickaite L, Mælandsmo GM, Seip K. 2022. AXL inhibition improves BRAF-targeted treatment in melanoma. *Sci Rep* **12:** 5076. doi:10.1038/s41598-022-09078-z

Ortiz R, Díaz J, Díaz N, Lobos-Gonzalez L, Cárdenas A, Contreras P, Díaz MI, Otte E, Cooper-White J, Torres V, et al. 2016. Extracellular matrix-specific Caveolin-1 phosphorylation on tyrosine 14 is linked to augmented melanoma metastasis but not tumorigenesis. *Oncotarget* **7:** 40571–40593. doi:10.18632/oncotarget.9738

Pandey V, Vijayakumar MV, Ajay AK, Malvi P, Bhat MK. 2012. Diet-induced obesity increases melanoma progression: involvement of Cav-1 and FASN. *Int J Cancer* **130:** 497–508. doi:10.1002/ijc.26048

Pascual G, Avgustinova A, Mejetta S, Martín M, Castellanos A, Attolini CS-O, Berenguer A, Prats N, Toll A, Hueto JA, et al. 2017. Targeting metastasis-initiating cells through the fatty acid receptor CD36. *Nature* **541:** 41–45. doi:10.1038/nature20791

Pohl J, Ring A, Ehehalt R, Herrmann T, Stremmel W. 2004. New concepts of cellular fatty acid uptake: role of fatty acid transport proteins and of caveolae. *Proc Nutr Soc* **63:** 259–262. doi:10.1079/PNS2004341

Pohl J, Ring A, Korkmaz U, Ehehalt R, Stremmel W. 2005. FAT/CD36-mediated long-chain fatty acid uptake in adipocytes requires plasma membrane rafts. *Mol Biol Cell* **16:** 24–31. doi:10.1091/mbc.e04-07-0616

Rabbani P, Takeo M, Chou W, Myung P, Bosenberg M, Chin L, Taketo MM, Ito M. 2011. Coordinated activation of Wnt in epithelial and melanocyte stem cells initiates pigmented hair regeneration. *Cell* **145:** 941–955. doi:10.1016/j.cell.2011.05.004

Rambow F, Rogiers A, Marin-Bejar O, Aibar S, Femel J, Dewaele M, Karras P, Brown D, Chang YH, Debiec-Rychter M, et al. 2018. Towards minimal residual disease-directed therapy in melanoma. *Cell* **174:** 843–855.e19. doi:10.1016/j.cell.2018.06.025

Rambow F, Marine JC, Goding CR. 2019. Melanoma plasticity and phenotypic diversity: therapeutic barriers and opportunities. *Genes Dev* **33:** 1295–1318. doi:10.1101/gad.329771.119

Riesenberg S, Groetchen A, Siddaway R, Bald T, Reinhardt J, Smorra D, Kohlmeyer J, Renn M, Phung B, Aymans P, et al. 2015. MITF and c-Jun antagonism interconnects melanoma dedifferentiation with pro-inflammatory cytokine responsiveness and myeloid cell recruitment. *Nat Commun* **6:** 8755. doi:10.1038/ncomss9755

Ring A, Le Lay S, Pohl J, Verkade P, Stremmel W. 2006. Caveolin-1 is required for fatty acid translocase (FAT/CD36) localization and function at the plasma membrane of mouse embryonic fibroblasts. *Biochim Biophysa Acta* **1761:** 416–423. doi:10.1016/j.bbalip.2006.03.016

Sandoval A, Chokshi A, Jesch ED, Black PN, Dirusso CC. 2010. Identification and characterization of small compound inhibitors of human FATP2. *Biochem Pharmacol* **79:** 990–999. doi:10.1016/j.bcp.2009.11.008

Sanna E, Miotti S, Mazzi M, De Santis G, Canevari S, Tomassetti A. 2007. Binding of nuclear Caveolin-1 to promoter elements of growth-associated genes in ovarian carcinoma cells. *Exp Cell Res* **313:** 1307–1317. doi:10.1016/j.yexcr.2007.02.005

Sensi M, Catani M, Castellano G, Nicolini G, Alciato F, Tragni G, De Santis G, Bersani I, Avanzi G, Tomassetti A, et al. 2011. Human cutaneous melanomas lacking MITF and melanocyte differentiation antigens express a functional Axl receptor kinase. *J Invest Dermatol* **131:** 2448–2457. doi:10.1038/jid.2011.218

Shao H, Teramae D, Wells A. 2023. Axl contributes to efficient migration and invasion of melanoma cells. *PloS one* **18:** e0283749. doi:10.1371/journal.pone.0283749

Sharma SV, Lee DY, Li B, Quinlan MP, Takahashi F, Maheswaran S, McDermott U, Azizian N, Zou L, Fischbach MA, et al. 2010. A chromatin-mediated reversible drug-tolerant state in cancer cell subpopulations. *Cell* **141:** 69–80. doi:10.1016/j.cell.2010.02.027

Smolle J, Woltsche I, Hofmann-Wellenhof R, Haas J, Kerl H. 1995. Pathology of tumor–stroma interaction in melanoma metastatic to the skin. *Hum Pathol* **26:** 856–861. doi:10.1016/0046-8177(95)90007-1

Sommer L. 2011. Generation of melanocytes from neural crest cells. *Pigment Cell Melanoma Res* **24:** 411–421. doi:10.1111/j.1755-148X.2011.00834.x

Tagawa A, Mezzacasa A, Hayer A, Longatti A, Pelkmans L, Helenius A. 2005. Assembly and trafficking of caveolar domains in the cell: caveolae as stable, cargo-triggered, vesicular transporters. *J Cell Biol* **170:** 769–779. doi:10.1083/jcb.200506103

Tsoi J, Robert L, Paraiso K, Galvan C, Sheu KM, Lay J, Wong DJL, Atefi M, Shirazi R, Wang X, et al. 2018. Multi-stage differentiation defines melanoma subtypes with differential vulnerability to drug-induced iron-dependent oxidative stress. *Cancer Cell* **33:** 890–904.e5. doi:10.1016/j.ccell.2018.03.017

Ubellacker JM, Tasdogan A, Ramesh V, Shen B, Mitchell EC, Martin-Sandoval MS, Gu Z, McCormick ML, Durham AB, Spitz DR, et al. 2020. Lymph protects metastasizing melanoma cells from ferroptosis. *Nature* **585:** 113–118. doi:10.1038/s41586-020-2623-z

Veeman MT, Slusarski DC, Kaykas A, Louie SH, Moon RT. 2003. Zebrafish prickle, a modulator of noncanonical Wnt/Fz signaling, regulates gastrulation movements. *Curr Biol* **13:** 680–685. doi:10.1016/S0960-9822(03)00240-9

Vivas-García Y, Falletta P, Liebing J, Louphrasitthiphol P, Feng Y, Chauhan J, Scott DA, Glodde N, Chocarro-Calvo A, Bonham S, et al. 2020. Lineage-restricted regulation of SCD and fatty acid saturation by MITF controls melanoma phenotypic plasticity. *Mol Cell* **77:** 120–137.e9. doi:10.1016/j.molcel.2019.10.014

Wang C, Jin H, Wang N, Fan S, Wang Y, Zhang Y, Wei L, Tao X, Gu D, Zhao F, et al. 2016. Gas6/Axl axis contributes to chemoresistance and metastasis in breast cancer through Akt/GSK-3β/β-catenin signaling. *Theranostics* **6:** 1205–1219. doi:10.7150/thno.15083

Weeraratna AT, Jiang Y, Hostetter G, Rosenblatt K, Duray P, Bittner M, Trent JM. 2002. Wnt5a signaling directly affects cell motility and invasion of metastatic melanoma. *Cancer Cell* **1:** 279–288. doi:10.1016/S1535-6108(02)00045-4

Widlund HR, Horstmann MA, Price ER, Cui J, Lessnick SL, Wu M, He X, Fisher DE. 2002. β-Catenin-induced melanoma growth requires the downstream target microphthalmia-associated transcription factor. *J Cell Biol* **158:** 1079–1087. doi:10.1083/jcb.200202049

Xu C, He J, Jiang H, Zu L, Zhai W, Pu S, Xu G. 2009. Direct effect of glucocorticoids on lipolysis in adipocytes. *Mol Endocrinol* **23:** 1161–1170. doi:10.1210/me.2008-0464

Yang W, Xia Y, Ji H, Zheng Y, Liang J, Huang W, Gao X, Aldape K, Lu Z. 2011. Nuclear PKM2 regulates β-catenin transactivation upon EGFR activation. *Nature* **480:** 118–122. doi:10.1038/nature10598

Yang P, Su C, Luo X, Zeng H, Zhao L, Wei L, Zhang X, Varghese Z, Moorhead JF, Chen Y, et al. 2018. Dietary oleic acid-induced CD36 promotes cervical cancer cell growth and metastasis via up-regulation Src/ERK pathway. *Cancer Lett* **438:** 76–85. doi:10.1016/j.canlet.2018.09.006

Zakut R, Perlis R, Eliyahu S, Yarden Y, Givol D, Lyman SD, Halaban R. 1993. KIT ligand (mast cell growth factor) inhibits the growth of KIT- expressing melanoma cells. *Oncogene* **8:** 2221–2229.

Zhang Z, Lee JC, Lin L, Olivas V, Au V, LaFramboise T, Abdel-Rahman M, Wang X, Levine AD, Rho JK, et al. 2012. Activation of the AXL kinase causes resistance to EGFR-targeted therapy in lung cancer. *Nat Genet* **44:** 852–860. doi:10.1038/ng.2330

Zhang M, Di Martino JS, Bowman RL, Campbell NR, Baksh SC, Simon-Vermot T, Kim IS, Haldeman P, Mondal C, Yong-Gonzales V, et al. 2018. Adipocyte-derived lipids mediate melanoma progression via FATP proteins. *Cancer Discov* **8:** 1006–1025. doi:10.1158/2159-8290.CD-17-1371

Zhou L, Liu XD, Sun M, Zhang X, German P, Bai S, Ding Z, Tannir N, Wood CG, Matin SF, et al. 2016. Targeting MET and AXL overcomes resistance to sunitinib therapy in renal cell carcinoma. *Oncogene* **35:** 2687–2697. doi:10.1038/onc.2015.343

Zoico E, Darra E, Rizzatti V, Budui S, Franceschetti G, Mazzali G, Rossi AP, Fantin F, Menegazzi M, Cinti S, et al. 2016. Adipocytes WNT5a mediated dedifferentiation: a possible target in pancreatic cancer microenvironment. *Oncotarget* **7:** 20223–20235. doi:10.18632/oncotarget.7936